

ECLIPSE

Efficient Cryogenic Low Invasive Propellant Supply Exchange

NASA Human Lander Challenge (HuLC) 2025

Theme: Advanced Cryogenics



Department of Aerospace Engineering
Grainger College of Engineering
University of Illinois Urbana-Champaign

Project Manager: Cliff Sun, Sophomore, Physics & Mathematics

Primary Advisor: Vishwanath Ganesan, Ph.D

Team Members

Aneesh Ganti*
Freshman
Computer Science, Mathematics

Braedyn Kim*
Freshman
Physics

Charles Cundiff**
Junior
Aerospace Engineering

Divij Garg**
Junior
Computer Science, Mathematics

Robert Barthell
Sophomore
Aerospace Engineering

Thach Dang
Freshman
Physics & Mathematics

John Galleta
Sophomore
Aerospace Engineering

Jett Haas
Sophomore
Physics

Keaton Jones
Sophomore
Aerospace Engineering

Justin Kotrba
Freshman
Aerospace Engineering

Anna Lambros
Freshman
Aerospace Engineering

Michael Milowski
Freshman
Aerospace Engineering

Sebastian Moreno
Freshman
Physics

Zahi Rahman
Freshman
Astrophysics

Sebastian Rojas
Freshman
Aerospace Engineering

Anna Rudenko
Freshman
Aerospace Engineering

Nate Vattana
Freshman
Aerospace Engineering

*Instrumentation Team Lead

**Propellant Transfer Team Lead

G. Vishwanath

Advisor signature indicating review & approval of submission





ECLIPSE: Efficient Cryogenic Low Invasive Propellant Supply Exchange

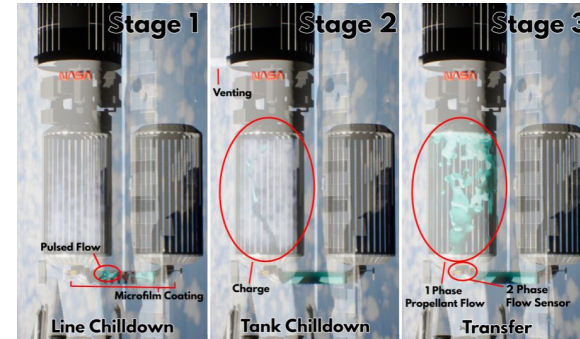
University of Illinois Urbana-Champaign



Theme Category, Major Objectives & Technical Approach

- Theme: Advanced Cryogenics
- Implement a low-cost, minimally invasive cryogenic transfer solution that is compatible across all spacecraft variants that require propellant transfer
- Address current gaps in NASA research in propellant transfer
- Mitigate propellant consumption and prioritize crew safety with transfer operations
- Reduce risk of tank over-pressurization during propellant transfer
- Optimize process of line chill-down and tank chill-down
- Advance NASA's two-phase flow monitoring technology

Concept of Operations:



Key Design Details

ECLIPSE utilizes a 3-stage process to transfer cryogenic propellant between tanks.

- Conduct transfer line chilldown with pulsed flow and microfilm coating.
- Utilize Charge-Hold-Vent (CHV) and No-Vent-Fill (NVF) to conduct tank chilldown and fill, transitioning based on a tank surface temperature measurements
- Measure void fraction and identify two-phase flow regimes during propellant transfer

Innovations

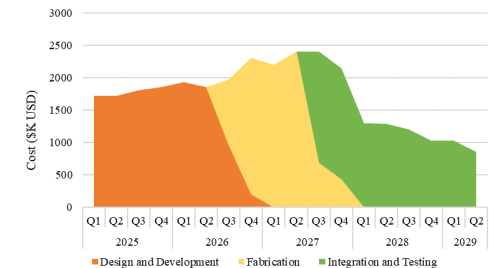
- Utilization of microfilm coating and pulsed flow to increase line chilldown efficiency
- Efficient and accurate void fraction and two-phase flow regime sensing in micro-gravity and reduced gravity environments
- Optimal temperature sensor location on the propellant tank surface and operational strategy for transition from CHV to NVF

Schedule

- Design and Development in FY 2025
- Technology completed in late FY 2026
- Fabrication and testing in FY 2027
- Precursor launch in early FY 2028
- Final testing and analysis in FY 2028-2029
- Final launch in late FY 2029

Costs

- Utilizing NICM, assuming upper bound cost of \$28.6M
- \$10M in design/development
- \$10.1M in fabrication
- \$8.5M integration and testing



Contents

I	Executive Summary	1
II	Introduction	1
III	System Overview	1
	III.A Developmental Timeline	1
	III.B Concept of Operations	2
IV	Line Chillover	3
	IV.A Pulse Flow	3
	IV.B Hydraulic Shock	4
	IV.C Inner Transfer Line Microfilm Coating	5
V	Two-Phase Flow Sensing	7
	V.A Sensor Overview	7
	V.B Sensor Components	8
	V.C Sensor Parameters	9
	V.D Flow Regime Identification Map	9
VI	Tank Chillover	11
	VI.A Charge-Hold-Vent and No-Vent-Fill Procedure	12
	VI.B Charge-Hold-Vent to No-Vent-Fill Transition	12
VII	Cost Analysis	12
VIII	Test Campaign	13
IX	Risk Analysis	14
X	Conclusion	14
XI	Acknowledgments	15
XII	Appendices	15
	XII.A Flow Boiling Background	15
	XII.B Hydraulic Shock Background	16
	XII.C GFSSP Modeling	17
	XII.D Tube Modification Trade Study	20
	XII.E Asymmetrical Sensor Visualization	22
	XII.F Sensor Parameters	22
	XII.G Sensor Accuracy Adjustment in Cryogenic Temperatures	22
	XII.H Tank Chillover Temperature Transition Calculation	23
	XII.I Sensor Materials Trade Matrix	24
	XII.J ANSYS Simulation Parameters	25
	XII.K Code	25



I. Executive Summary

Cryogenic propellant boil-off during propellant transfer threatens mission longevity and Human Landing System integrity by depleting available propellant and increasing the risk of over-pressurization. The Efficient Cryogenic Low Invasive Propellant Supply Exchange (ECLIPSE) architecture addresses these challenges by controlling and monitoring propellant boil-off during chilldown and transfer. During line chilldown, a periodic pulse flow, optimized to reduce hydraulic shock, and microfilm pipe coatings minimize propellant boil-off. During tank chilldown, Charge-Hold-Vent (CHV) and No-Vent-Fill (NVF) operations minimize tank over-pressurization and unintended propellant venting. The CHV-NVF transition is reliably triggered by measuring tank temperatures. To monitor transfer, a low-invasive capacitance sensor reliably identifies two-phase flow boiling regimes and measures void fraction along the transfer line. By minimizing propellant consumption, reducing tank over-pressurization, and monitoring microgravity two-phase flow physics during transfer, ECLIPSE advances cryogenic fluid management technologies in support of long-duration Artemis missions and sustained deep space exploration.

II. Introduction

The University of Illinois at Urbana-Champaign proposes the Efficient Cryogenic Low Invasive Propellant Supply Exchange (ECLIPSE), a comprehensive and holistic propellant transfer architecture designed to advance Cryogenic Fluid Management (CFM) for NASA's Artemis missions. Advancing CFM technologies is critical for sustaining long-duration human exploration beyond Low Earth Orbit (LEO) [1]. Due to the extremely low storage temperatures of cryogenic propellants, flash boiling is induced by direct contact with HLS architecture such as pre-chilled cryogenic transfer pipes and storage tanks. Flash boiling generates boil-off, which actively reduces usable liquid propellant and increases the risk of tank over-pressurization. To address these challenges, ECLIPSE actively manages and mitigates boil-off risks, significantly enhancing safety and efficiency from the moment the transfer line is established through the transition to stable, single-phase cryogenic transfer. Specifically, ECLIPSE minimizes propellant losses during line chilldown, reduces the risk of over-pressurization during tank chilldown, and continuously monitors microgravity two-phase propellant flow regimes in real time. The system is designed to be compatible with all spacecraft variants that require cryogenic propellant transfer. ECLIPSE's system requirements are listed in Table 1 in compliance with the Human Lander Challenge (HuLC) guidelines. Note, single-phase flow is defined as the movement of a single fluid phase of either pure liquid or pure vapor. Two-phase flow is defined as a simultaneous flow of both the liquid and vapor phases of the propellant. For clarity within this paper, single-phase flow refers exclusively to the movement of a pure liquid, while two-phase flow denotes the simultaneous flow of liquid and vapor phases.

Table 1 ECLIPSE System Requirements

Identifier	Requirement
MR-01	ECLIPSE shall mature advanced Cryogenic Fluid Management technologies.
MR-02	ECLIPSE shall be capable of implementation in ≤ 5 years.
MR-03	ECLIPSE shall function in a microgravity environment.
MR-04	ECLIPSE shall have a mission operational lifespan of ≥ 3 months.

III. System Overview

A. Developmental Timeline

The developmental timeline for ECLIPSE begins in the Fiscal Year (FY) 2025 with a Mission Concept Review to outline the mission architecture and examine the proposed objectives. System Requirements and Mission Design Reviews are scheduled during FY 2025 and 2026, respectively, to verify mission design and requirements. The Preliminary and Critical Design Reviews are scheduled in FY 2026 and 2027



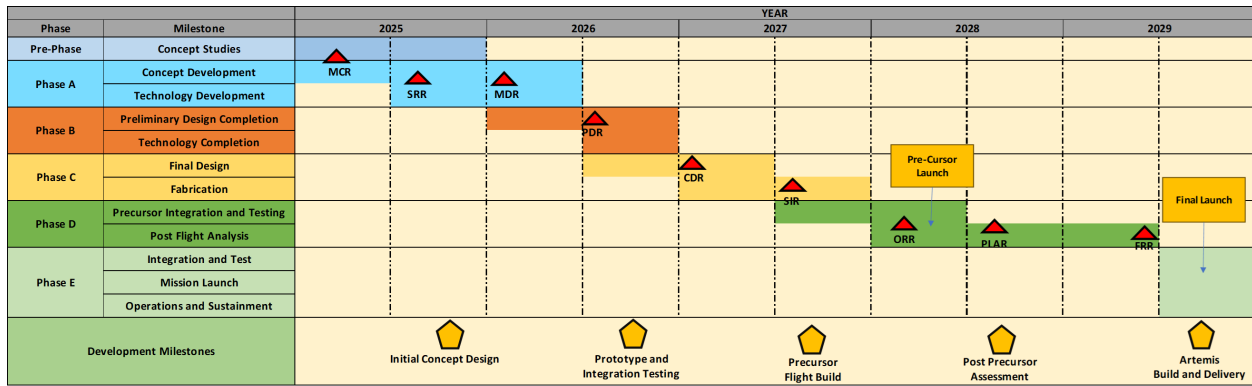


Fig. 1 ECLIPSE Mission Timeline

respectively, leading to fabrication. Integration and testing are scheduled during FY 2027 and FY 2028, culminating in a precursor launch in Q2 of FY 2028 which will test system integration. Following the precursor launch, a Post Launch Assessment Review is conducted to refine system integration and testing for future deployments. ECLIPSE is intended to launch in Q4 of FY 2029. This timeline was largely influenced by NASA’s Cryogenic Fluid Management Technology development roadmap [2]. The schedule is slightly delayed from the preliminary timeline in the earlier ECLIPSE proposal. The additional time between the precursor launch and the first full operation of ECLIPSE allows for any issues with integration and operation to be resolved.

B. Concept of Operations

ECLIPSE’s operations begin once the cryogenic propellant transfer line is established between HLS and a fuel depot. A fuel depot is a spacecraft designed for HLS propellant resupply. Stage 1 is the transfer line chilldown using the cryogenic propellant itself. To maximize line chilldown efficiency, that is minimizing propellant consumption, a combination of pulse flow fluid operations and microfilm line coatings are leveraged. The valve closing time for pulsed flow will be prolonged to mitigate hydraulic shock. Stage 2 is the initial tank chilldown. To minimize the risk of tank over-pressurization and reduce unintended propellant venting, ECLIPSE leverages Charge-Hold-Vent (CHV). CHV is the process of repeatedly injecting a propellant charge into the receiving storage tank and waiting for complete charge boil-off, stopping when the tank is sufficiently cooled. When the maximum surface temperature of the tank is below a temperature threshold, venting shuts off and propellant transfer initiates, beginning No-Vent-Fill (NVF). Stage 3 is the single-phase liquid propellant transfer into the storage tank. During this stage, ECLIPSE’s low-invasive two-phase flow sensor monitors the propellant flow by identifying two-phase flow regimes and measuring void fraction at the end of the transfer line. The concept of operations are depicted in Fig. 2.

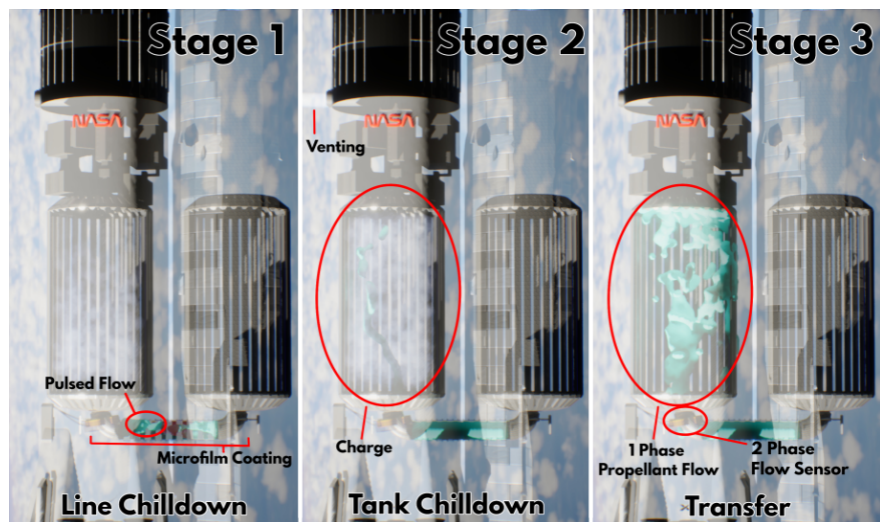


Fig. 2 ECLIPSE’s Concept of Operations

During this stage, ECLIPSE’s low-invasive two-phase flow sensor monitors the propellant flow by identifying two-phase flow regimes and measuring void fraction at the end of the transfer line. The concept of operations are depicted in Fig. 2.

IV. Line Chillover

For successful cryogenic propellant transfer, the propellant transfer line must be chilled down to cryogenic temperatures. The simplest and most energy efficient method is to use the propellant itself for cryogenic line chillover [3]. Due to the extreme initial temperature difference between the cryogenic propellant and the tube, a thin superheated vapor film initially exists between the wall and the liquid. This regime, known as inverted annular film boiling, insulates and reduces heat transfer. Nucleate boiling, with its higher heat flux, is desirable but occurs at a lower temperature difference. Line chillover efficiency (Eq. 2 in Appendix XII.A) is the ratio of heat removed from the transfer line to the heat removal capacity of the propellant fluid. Chillover efficiency is dependent on flow boiling characteristics, which can be modified in a variety of ways. A new pulse flow control system and a low thermal conductive coating along the inner surface of the transfer line are proposed to mitigate film boiling.

A. Pulse Flow

In pulse flow, the inlet valve is cyclically opened and closed with a consistent duty cycle and pulse width until chillover is achieved to ensure the transfer of useable liquid propellant. The sudden appearance and subsequent absence of the liquid destabilizes the liquid-vapor interface in the inverted annular film boiling regime [4]. The quiescent time between pulses also gives the vapor more time to absorb the pipe's heat compared to continuous flow. While pulse flow typically takes longer to complete compared to constant trickling, overall it consumes less propellant in the process. The degree of the line chillover efficiency depends on the pulse length [5]. Propellant mass savings of 30% in microgravity, however, have been observed with just the addition of pulse flow [3]. Importantly, pulse flow improves chillover efficiency without adding considerable mass to the system. To evaluate the impacts of pulse flow, NASA's Generalized

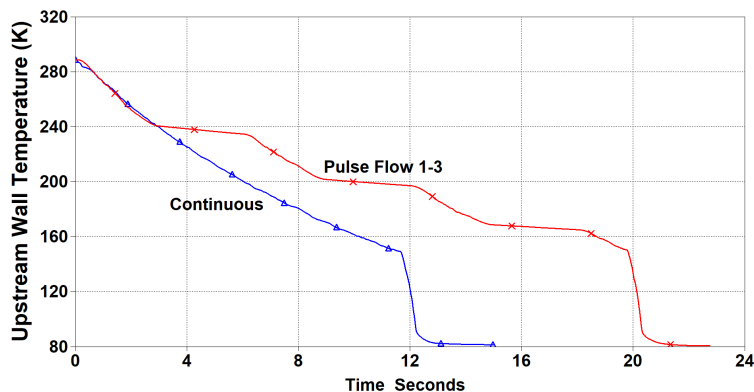


Fig. 3 The upstream wall temperature is depicted for pulse flow (red) and continuous flow (blue). While pulse flow takes longer to chill, it uses significantly less propellant.

Fluid System Simulation Program (GFSSP) [6] can be used. In this program, a nodal model be configured to model a variety of fluids systems. The model generated by LeClair [7] was used as a baseline and a pulse flow element was added to compare the performance of continuous flow to pulse flow. Heat correlations from [8] were implemented in this model to accurately represent cryogenic chillover. For more information on the model used, reference Appendix XII.C.

The results of this simulation are depicted in Figs. 3 4. As seen in Fig. 3, continuous flow results in a faster decrease in wall temperature. Figure 4 shows the total mass consumed to chill down the upstream node, which is the first solid node in the model. The simulated mass savings of roughly 20% are consistent with results in the literature. It is clear that lower valve duty cycle result in decreased amount of propellant used. The cryogenic propellant has more time to transfer heat during quiescent periods and so more of its latent heat is transferred. This reduces the overall consumption due to more efficient use. Lower duty cycles should be balanced with an increase in time to chill, which increases as duty cycle decreases.

While pulse flow decreases propellant consumption, it also can increase valve degradation [3]. Valve

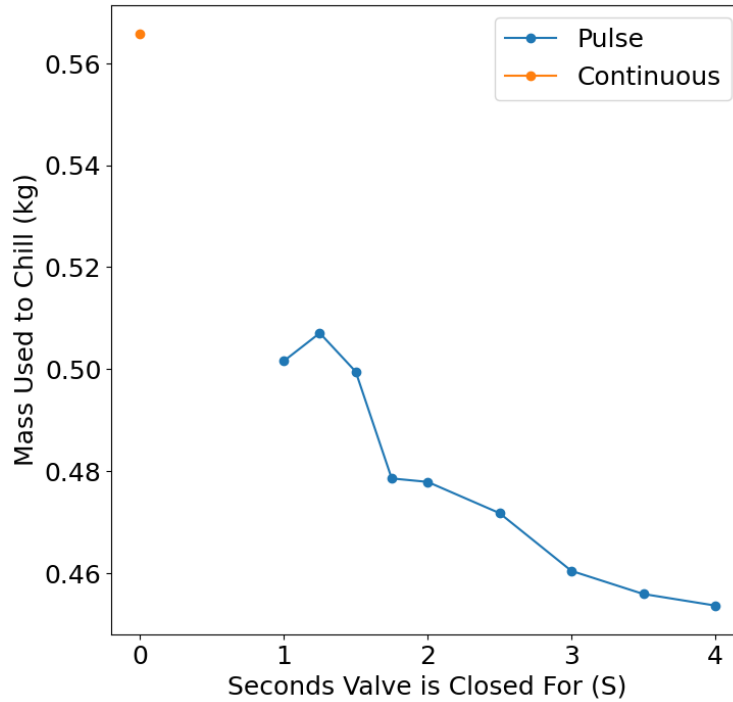


Fig. 4 Total propellant used to chill the upstream node is compared for various 1-X open-close pulse configurations and continuous flow.

malfunction may disrupt the chilldown process and lead to over-pressurization, causing more propellant to be consumed and potentially damaging HLS architecture. To minimize this risk, an emphasis will be placed on selecting cryogenic-rated lubricants, implementing valve pre-chill procedures to minimize thermal shock, and conducting rigorous valve cycling tests during the testing and integration phase. This ensures the reliability of the valve system when performing pulse flow.

B. Hydraulic Shock

Pulse flow also induces transient hydrodynamic effects as a result of its unsteady nature. These fluid disturbances move throughout the system and potentially damage components. Current research has not focused on the effects of fluid transients in microgravity. These effects present a lower danger at small experimental scales, but must be understood and mitigated to prolong lifetime if implemented in HLS. The primary fluid transient effect is hydraulic shock, characterized by a moving pressure wave. Changing the valve action time is the best method to mitigate the pressure spike. See Appendix XII.B for more information on hydraulic shock. While increasing the valve closure time will reduce the magnitude of hydraulic shock, it may also have effects on pulse flow. Without sudden starts and stops, pulse flow becomes less effective at destabilizing the thin vapor film. Therefore, a valve action time must be found that mitigates pressure transients while maximizing the benefits of pulse flow.

To more accurately model the fluid system and find an optimal valve closure time, GFSSP is again used [6]. This software has been used to model the transient effects of hydraulic shock [9]. For more information on the model, reference appendix XII.C. Figure 5 depicts the maximum pressure measured adjacent to the valve with various open and close times. Clearly, decreasing the close time of valves has a significant effect on the magnitude of hydraulic shock. Changing the valve open time, however, has almost no effect on the pressure spike's magnitude. The optimal valve open time for pulsed flow is therefore as fast as possible. To decide on an optimal valve closing time, which is largely responsible for hydraulic shock, the pressure ratings of all components and sensors in the system must be known. Stresses from pulse flow will also be

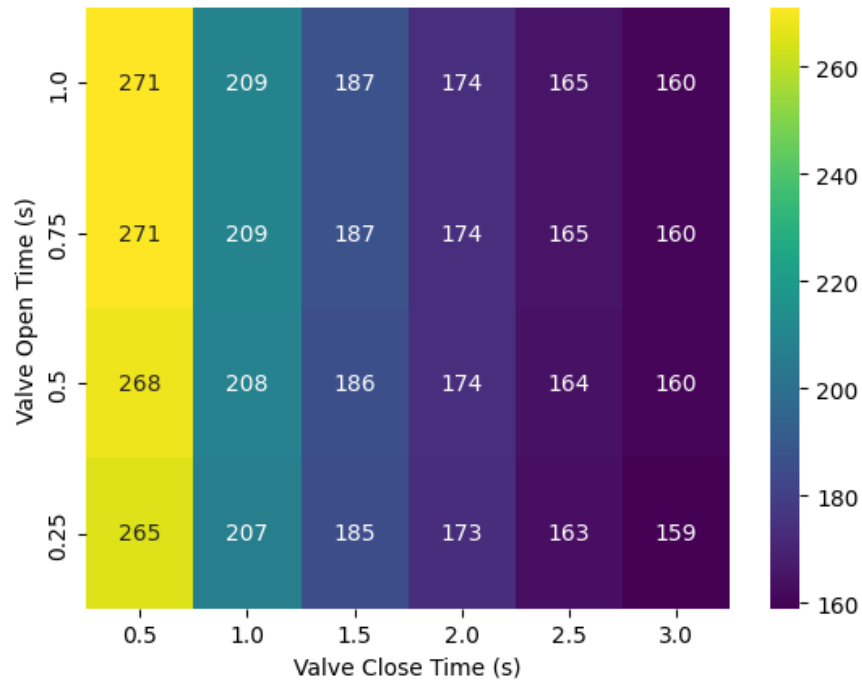


Fig. 5 This figure depicts the maximum measured pressure for various valve open and closing times for a 60' length of tube.

cyclical, complicating any calculations made to identify a singular optimal closing time. As seen in Fig. 5, lengthening the valve closure time gives diminishing returns while degrading the benefits of pulsed flow. To stay on the safe side, a closing time can be chosen that creates a pressure transient no larger than twice the nominal pressure, which is 120 psi in this simulation. With this rule, a valve close time no longer than two seconds should be used. Operational changes can reduce the damaging effects of hydraulic shock during pulse flow. Optimizing a more accurate simulation like this can mitigate the potential complications of pulse flow while maximizing its benefits. This analysis reduces the uncertainties associated with pulse flow and makes the technique more viable for use on HLS.

C. Inner Transfer Line Microfilm Coating

Modifying the transfer line inner surface can increase chilldown efficiency, reduce chilldown time, and minimize propellant boil-off. A comprehensive trade study (Tables 3, 4 in Appendix XII.D) was conducted to compare various tube modifications. Microfilm coatings, micro-fins, capillary coatings, surface etching, and microstructures were investigated. Five characteristics were used in the comprehensive trade matrix. Technology Readiness Level (TRL) and Manufacturing Readiness Level (MRL) were selected to emphasize the importance of maintaining a low cost and short timeline of integration. Heat transfer enhancement was considered to measure the effectiveness of the coating during propellant transfer. Observed pressure fluctuation and estimated durability were selected to minimize impact on fluid flow and maximize effective lifespan.

Microfilm coatings are made up of low thermal conductivity polymers that influence the chilldown process. Tested during parabolic flight, microfilm coatings demonstrate good results compared to bare tubing in a microgravity environment [10]. Research has shown that this coating can increase chilldown efficiency by up to 176% and produce a 65% reduction in boil-off over the entire chilldown. The microfilm coating improved performance at a variety of coating thicknesses and inlet conditions, showing an average chilldown efficiency increase of roughly 100% [11]. Microfilm coatings had the highest TRL, MRL, and estimated durability of those examined. They also produce no observed pressure fluctuations and have similar heat

transfer enhancement to competing surface modification techniques. Microfilm coatings were found to be the ideal tube modification and are proposed as part of ECLIPSE's line chilldown solution.

The impact of microfilm coatings on chilldown efficiency can be analyzed in two primary phases: during film boiling regime and during transition and nucleate boiling post rewetting. First, the insulation provided by the microfilm affects the initial cooling of the transfer line. The microfilm layer insulates the inner tube surface from the bulk mass of the tube, allowing the inner surface to reach cryogenic temperatures while the tube is still warm. This facilitates early transition from film boiling to nucleate boiling, enhancing overall chilldown efficiency. In contrast, the second effect of microfilm coatings on the chilldown process is the reduction in heat transfer. The microfilm coating, owing to its poor thermal conductivity, reduces the heat conduction from the tube to the fluid once nucleate boiling is reached. Balancing these two competing effects is critical for maximizing thermal performance during a chilldown.

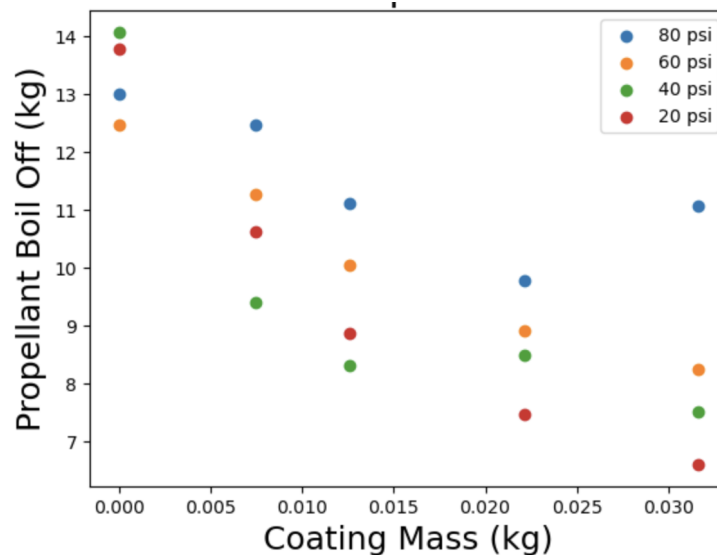


Fig. 6 Propellant mass saved compared to FEP coating mass added for 0, 1, 2, 3, and 4 layers of microfilm coating and various pressures. Data was taken from experimental low gravity tests [12].

To explore this balance, the expected amount of propellant saved per mass added per meter of 10 inch tubing for various coating thicknesses is calculated in Figure 6. These results were derived using Eqs. 2-8 to calculate the coating's mass and cryogenic chilldown efficiency data [12]. It is clear from the figure that the initial layers of coating provide a large benefit while later coatings provide diminishing returns. It is also evident that the microfilm coating provides greater benefits at low pressures and low mass flow rates [12]. Nonetheless, microfilm coatings provide significant mass savings even when used least optimally for small mass cost.

Another key logistical concern is if the coating can be easily and cost-effectively applied. In multiple studies, the coating has been applied through the pour and drain process [11]. A pour and drain process, however, would require much more coating material at larger scales and can create uneven coats. For a larger application, fluorinated ethylene propylene (FEP) can also be sprayed onto the surface and then cured [13]. Machines that evenly spray coat the inner tubes of larger pipes already exist and are used in the oil and gas industry. The tubes can then be cured in specialized ovens. This manufacturing process is scalable and will make integration into HLS relatively simple and cheap.

One last concern is the exact material used for the microfilm coating. The fluoropolymer coatings considered for this application are Fluorinated Ethylene Propylene (FEP) and Polytetrafluoroethylene (PTFE). Both offer distinct advantages depending on the operational context. FEP and PTFE exhibit significant dimensional shrinkage at cryogenic temperatures. FEP has a lower thermal expansion coefficient (CTE) in the range of $82 - 104 \times 10^{-6} \text{ m/mC}$ compared to PTFE's higher range of $99 - 151 \times 10^{-6} \text{ m/mC}$. A typical substrate

is Stainless Steel with a CTE of 17.3×10^{-6} . As FEP better matches the CTE of its substrate, FEP-coated will experience fewer shrinkage problems. PTFE and FEP demonstrate similar temperature ranges of -260°C to 260°C and -268°C to 205°C respectively [14]. FEP offers greater diversity in application methods through its melt-processability. This characteristic enables uniform coatings on complex geometries without extensive post-processing, while PTFE typically necessitates machining or tape application. Mechanically, PTFE provides enhanced resistance to creep deformation and abrasive wear. FEP is advantageous due to its combination of CTE better matching SS and superior adaptability in coating methods positions FEP as the preferred fluoropolymer for ensuring stable performance in cryogenic systems[15].

GFSSP can also be used to model the effects of microfilm coating on tube chilldown. The LeClair model [7] was again used as a baseline and a second layer of solid nodes representing the microfilm coating was added. Data for the microfilm's cryogenic thermal properties were found from NIST [16]. It should be noted that this result was created with Miropolski heat correlations. Results of this simulation are depicted in Fig. 7. In these simulations, the coated transfer line chills down faster and more efficiently than the uncoated transfer line.

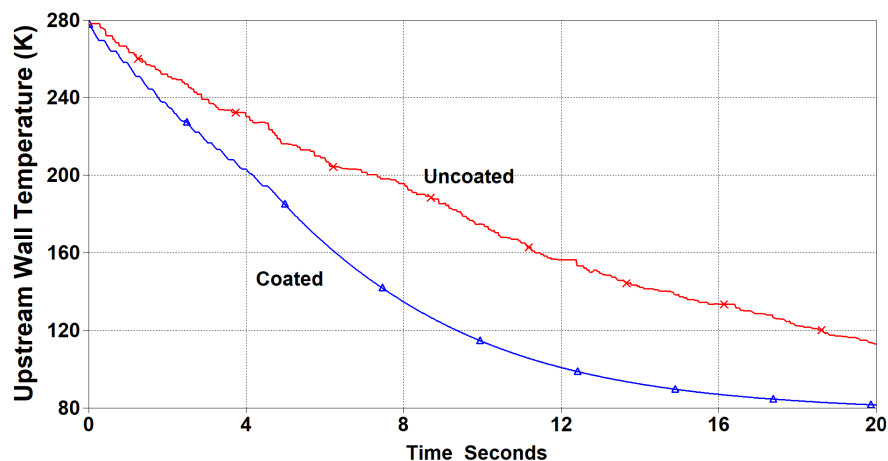


Fig. 7 Chilldown curves for microfilm (blue) and non-microfilm (red) show that microfilms decrease chilldown time.

The efficiency gains of microfilm coatings are primarily due to the insulation between the inner surface and the tubes bulk, resulting in the system reaching the Leidenfrost point faster as the microfilm surface nodes chill down faster. Thus, the heat regime focuses more on the more efficient nucleate boiling phase. A detailed description of the model is given in Appendix XII.C.

Microfilm coatings provide both time and mass savings during line chilldown evidenced experimentally and in simulation by our model. Microfilm coatings add little mass to the system and can be integrated easily into the HLS system. They are a net benefit for the system and are used as part of the ECLIPSE proposal.

V. Two-Phase Flow Sensing

Accurately monitoring cryogenic propellant transfer and line chilldown is necessary to gauge chilldown efficiency and transfer health. Existing propellant transfer sensing techniques, such as radio [17], probe [18], and fiber optic [19], are limited by unreliable measurements in microgravity and/or system-level integration incompatibility. To bridge these gaps, an accurate, low-invasive, gravity-independent capacitance sensor is proposed.

A. Sensor Overview

The capacitance sensor, to be integrated along the transfer line as seen in Stage 3 of the Concept of Operations in Fig. 2, measures void fraction and identifies two-phase flow boiling regimes to monitor

chilldown efficiency and transfer health. The sensor generates an electric field between two fixed electrodes to extract the capacitance of the two-phase fluid. The measured time-domain capacitance signal between the electrodes is then used to calculate the void fraction of the two-phase fluid [20] and identify the two-phase flow regime [21].

An initial linear approximated relationship between the void fraction and capacitance can be determined from the following parameters: C_L which is the capacitance of the liquid, C_G which is the capacitance of the gas, and C_M which is the measured capacitance. C_L and C_G can be calculated based on the electrode configuration, the medium relative permittivity of the cryogenic propellant ϵ , and the vacuum permittivity ϵ_0 . C_L , C_G , and C_M can be used to calculate a naive linear void fraction: $\alpha_{linear} = (C_L - C_M)/(C_L - C_G) \times 100\%$.

Calibration is required to get an accurate void fraction function as a function of the measured capacitance value. This is typically done using Finite Element Method (FEM) simulations based on sensor geometry [22, 23]. The first step in calibration is to input the sensor geometry as the simulating parameters. Then, FEM can be used to generate void fraction points based on an inputted capacitance value, where the capacitance values will be dependent on the sensor geometry and fluid parameters. A non-linear curve can be fitted to these coordinate points, creating a void fraction relation as a function of capacitance. This new calibration curve can then be experimentally verified using data collected from suborbital flights in the ECLIPSE test campaign. An example of a corrected equation is shown in [20], where a constant k was introduced where k is proportional to the distance between the electrodes.

$$\alpha_{corrected} = k\alpha_{linear}^2 + (1 - 100k)\alpha_{linear} [\%] \quad (1)$$

In parallel with the void fraction calculation, three statistical parameters are drawn from the time-resolved capacitance signal. These parameters are the time-averaged mean of the capacitance signal, the time domain variance of the signal, and the kurtosis of the signal. Kurtosis is defined as the 4th statistical central moment divided by σ^4 . Note, these 3 statistical parameters differ from the proposal paper. It is important to note that choosing a fixed time interval Δt is necessary to calculate the statistical parameters. This Δt can be programmed depending on the integrated system requirements.

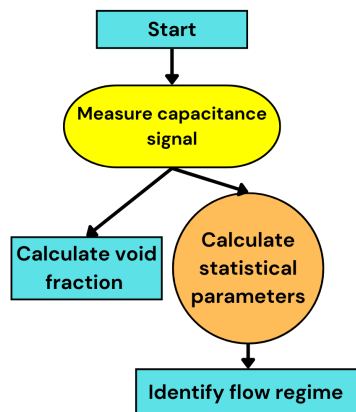


Fig. 9 Sensor Steps

the flow path.

This sensor is to be integrated at the end of the transfer line pipe, near the receiving tank. The total

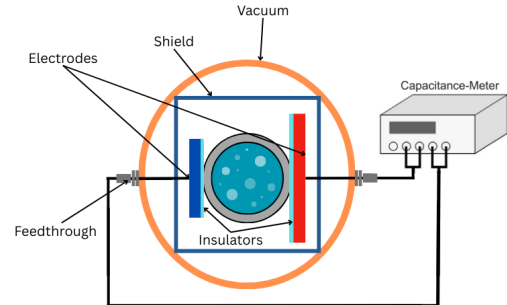


Fig. 8 Capacitance Two-phase Flow Sensor Example

The sensor's algorithm, shown in Fig. 9, is as follows. First, the sensor will measure and analyze the capacitance signal to derive the void fraction and the three statistical parameters. The sensor will then utilize a pre-existing three-dimensional flow regime identification map to map the capacitance mean, variance, and kurtosis to a specific flow regime.

B. Sensor Components

An asymmetrical capacitance sensor is proposed, which uses parallel, flat, anti-symmetric electrodes. That is one electrode's length and width is longer than that of the other. The electric field flows from the longer, high-potential electrode to the smaller, low-potential electrode. An asymmetric capacitance sensor reduces the electric field curvature from one electrode to the other compared to other sensor types [24]. Notably, other sensor geometries lose information about the electric field due to field curvature, leading to inaccurate capacitance readings. The visualization models in Appendix XII.E show how the generated electric field fully encompasses

estimated mass of the system will be 25kg. The electrodes will be made of copper, which will then be surrounded by insulators. It is important to note that a good electrode insulator permits the electric field to propagate through the stainless steel pipes with minimal interference (as to not impact capacitance measurements). To determine the electrode insulator, a trade study was done on various insulation materials, as see in Appendix XII.I. From this trade study, X-Aerogel was chosen as the electrode insulator.

In addition to the electrode insulator, a sensor shield is required to minimize interference with sensor measurements. To determine the shield material, a trade study was done on various shield materials, as seen in Appendix XII.I. From this trade study, aluminum was chosen as the sensor shield. If the pipe is vacuum jacketed, a hermetic vacuum feedthrough can be used to connect the sensor to an external capacitance meter that is living outside the transfer line. Cryogenic temperatures also affect the sensor accuracy, which ECLIPSE accounts for in Appendix XII.G.

C. Sensor Parameters

The sensor's high level parameters can be seen in Fig. 10. The minimum frequency that the sensor operates at is 200 Hz, which is twice the highest frequency component of 100 Hz for any measured capacitance signal as reported by [20]. Note, the highest frequency component can be determined by taking a Fourier Transform of the time-domain capacitance signal, then locating the largest frequency of which the magnitude of the Fourier transformed signal is not zero. This minimum sensor operational frequency was chosen based on the Nyquist theorem, which states that a periodic signal must be sampled at more than twice the highest frequency component of the signal [25].

Requirement	Value
Sampling Frequency	≥ 200 Hz
Excitation Frequency	10 Hz (Can burst to 1 kHz)
System Power	~ 10 W
Potential Difference	25 V
Estimated Total Mass	25 kg

Fig. 10 High Level Sensor Parameters

It is also important to note that the sensor's operational frequency exceeds the 100 Hz minimum adopted in NASA's 2023 parabolic-flight ECT experiment [26]. Further details on the sensor parameters can be seen in Appendix XII.F

D. Flow Regime Identification Map

Although void fraction measurements provide valuable insight into the processes within the transfer line, they alone cannot fully characterize the complex nature of flow boiling regimes. Accurate identifica-

tion of these regimes is crucial for comprehensive understanding of the behavior of cryogenic propellants during transfer operations. Previous experimental work demonstrated that the statistical characteristics of the time-resolved capacitance signals in the time and frequency domains could effectively distinguish between flow regimes [21]. However, practical constraints such as limited microgravity duration during parabolic or sub-orbital flights severely restrict the collection of adequate capacitance data points. Consequently, traditional Fourier analyses, which depend on extensive datasets, are not viable in these short-duration scenarios.

Additional work explored flow regime mapping using non-cryogenic fluids [27]. However, these approaches were developed specifically for water and similar fluids and relied on prior knowledge of fluid properties, such as liquid and gas viscosities and densities. These two fluid properties were then used to calculate a single parameter called the Suratman number, which was intended to help distinguish flow regimes. However, distinguishing flow regimes solely with the Suratman number often exhibited overlapping different regimes corresponding to the same Suratman number. This reduces the effectiveness of the Suratman number being a unique identifier of flow regimes. Moreover, such fluid parameters (viscosity and density) may not always be readily available or accurately measurable in cryogenic applications. These gaps highlights the necessity for robust, adaptable techniques of flow regime identification that is both independent of fluid-specific properties and whose parameter space is larger than one dimension.

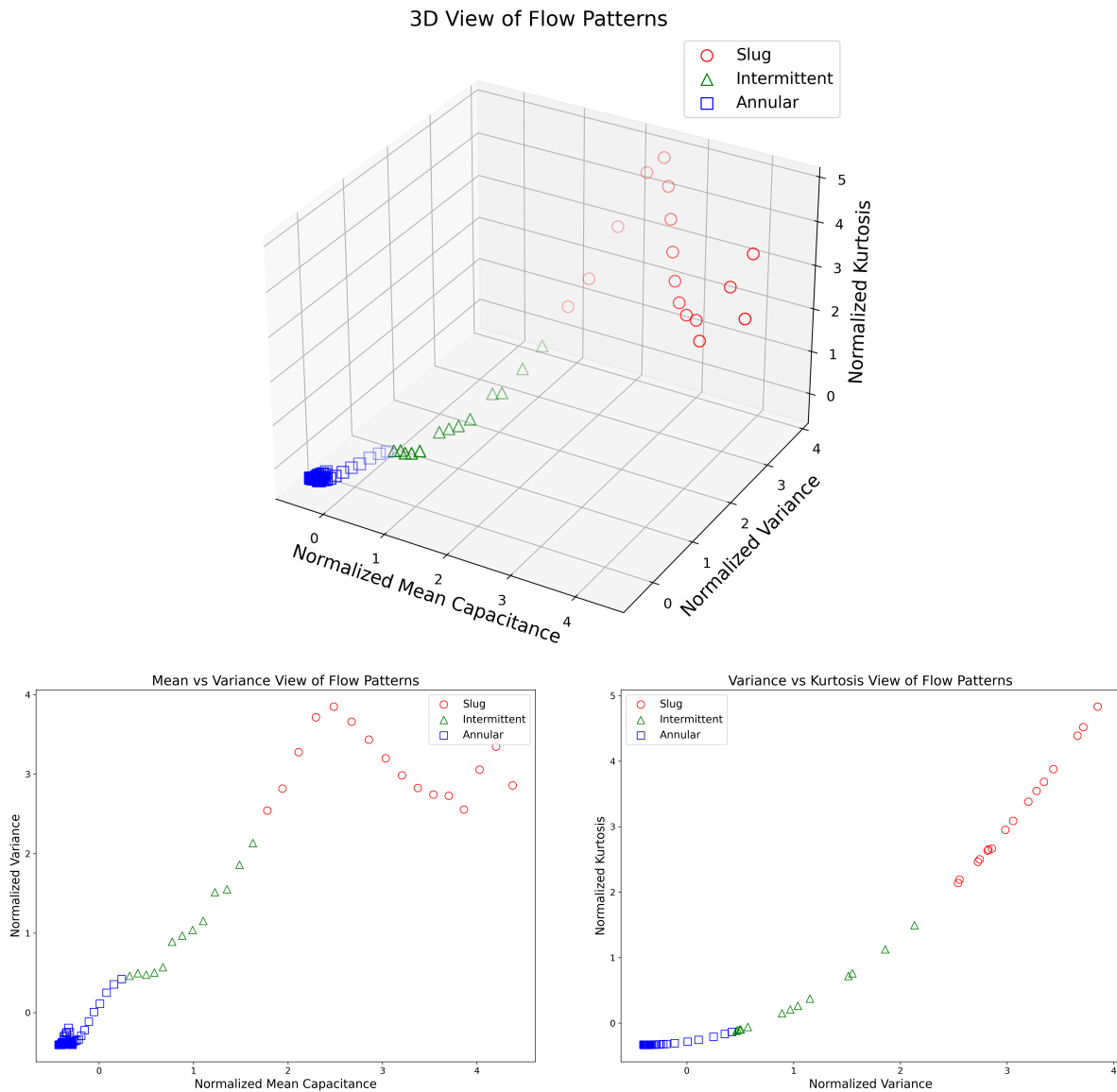


Fig. 11 Generated 3D Flow Regime Map

To overcome the constraints posed by limited microgravity durations, we propose leveraging different parameters for flow regime classification. As an initial proof of concept, the fluid dynamics simulation software ANSYS was selected to simulate two-phase flow boiling regimes due to its robust capabilities in accurately modeling complex fluid dynamics. A comprehensive list of ANSYS simulation parameters are detailed in the appendices XII.J. The simulation process begins by measuring the cross-sectional void fraction. This measured void fraction is then converted to a capacitance signal through an established linear relationship, iteratively reconstructing a complete time-resolved capacitance profile for each flow regime. Although simulations were performed under gravity conditions, previous research [28] indicates that flow regimes observed in gravity are consistent with those observed under microgravity. Thus, the flow regime map generated under gravity conditions serves as a robust proof of concept, supporting the applicability of the technique to microgravity conditions. Leveraging future microgravity simulations with high Technology Readiness Levels (TRL) will further simplify flow regime map construction.

Given the brief durations of microgravity flights, datasets often exhibit imbalances, with some flow regimes having fewer data points than others. To address this challenge, a machine learning-based time-series

model is employed to extend existing capacitance data and to close any large data point gaps between flow regimes. For this simulation, the number of data points for slug and intermittent was doubled, while that of annular remained the same because of the imbalance of data points for slug, intermittent, and annular. The consistent seasonal patterns observed in the capacitance signal within the time domain ensured that the time-series extension did not result in over-extrapolation.

To reliably identify and classify different flow regimes, candidate statistical parameters were rigorously evaluated. In particular, statistical moments, which are most commonly used to classify the shape of any arbitrary probabilistic distribution, were assessed. A criterion was established to evaluate the distinctiveness of flow regime clusters, focusing specifically on the separation of centroids with the highest probability between slug, annular, and intermittent regimes. Based on this analysis, three central statistical moments were selected: mean (first moment), variance (second moment), and kurtosis (fourth moment). These parameters demonstrated the strongest ability to distinguish clearly between flow regimes.

Subsequently, the time-resolved capacitance signals were segmented into intervals defined by a carefully selected interval duration (Δt). Selecting a larger Δt enhances the accuracy of the parameters but decreases the spatial resolution of the flow regime map. In contrast, reducing Δt increases spatial resolution but may compromise the accuracy of the parameters. The team chose a $\Delta t = 0.1$ seconds, which resulted in each group having 10 points. Selecting a $\Delta t > 0.1$ resulted in little change in the distribution of the flow regime map.

To complete the construction of the flow regime map, a probabilistic clustering algorithm was implemented, specifically Fuzzy c-means. This algorithm groups data points into probabilistic clusters, assigning membership values to each point in multiple clusters using distance metrics and probability scores. Each cluster is represented by a centroid that is calculated as the average of all points within the cluster. This final step allows the creation of a detailed three-dimensional flow regime map at the cost of lesser points on the map.

Figure 11 illustrates a representative three-dimensional visualization of the generated flow regime map. Preliminary results indicate clear and distinct clusters corresponding to the slug, annular, and intermittent flow regimes, demonstrating the effectiveness and robustness of the proposed approach. Furthermore, the flexibility of this method allows easy integration of additional flow regimes by simply expanding the clustering model to include more clusters. This structured and adaptable mapping technique presents a significant advancement in flow regime identification, supporting robust and precise monitoring of cryogenic propellant transfers under varying operational conditions.

Artemis Science Objectives	Human Landing System Goals		ECLIPSE Goals	Science Objectives	Scientific Measurement Requirements		Mission Requirement
					Measured Parameters	Observables	
Advance the development and demonstration of long-duration cryogenic fluid storage and transfer technologies in space	On-Orbit Cryogenic Propellant Transfer	Design a secure and efficient method for transferring cryogenic propellant during the line and tank chilldown	Monitor 2 phase-flow along transfer lines	Measure characteristics of 2 phase-flow	Capacitance	Void Fraction	ECLIPSE Phase 1-3
					Capacitance	Flow Regimes	

Fig. 12 Instrumentation System Requirements

VI. Tank Chilldown

Tank chilldown is necessary for propellant to be transferred to the final storage tank. Chilldown can be achieved by boiling off propellant or cryo-coolers, though their lack of scalability and high energy consumption makes integration on HLS unfeasible [29]. While a focus of line chilldown is to minimize propellant loss, tank chilldown is primarily concerned with reducing the risk of over-pressurization caused by the expansion of boiled-off cryogens. In terrestrial gravity, tank chilldown can be performed with a top vent held open as gravity stratifies the liquid from the gas. In microgravity conditions, however, there is an additional risk of unintentionally venting propellant due to unknown liquid positions within the tank.

Venting liquid directly reduces performance and could impart unexpected forces on the spacecraft. To minimize the risk of over-pressurization and venting liquid cryogen, ECLIPSE proposes Charge-Hold-Vent and No-Vent-Fill.

A. Charge-Hold-Vent and No-Vent-Fill Procedure

Charge-Hold-Vent (CHV) is the first phase of tank chilldown and prepares the tank for single-phase liquid cryogenic propellant transfer. The process begins by injecting one propellant charge into the tank with vents closed. Once the propellant has fully boiled-off, it is completely vented. These steps are repeated until the tank is sufficiently cold. By venting boil-off propellant, CHV mitigates the risk of over-pressurization. Furthermore, venting only occurs once the entire propellant charge has boiled off, minimizing the risk of unintended liquid propellant venting. After CHV has sufficiently cooled down the tank, single-phase cryogenic propellant is transferred into the storage tank with vents shut off in a process called No-Vent-Fill (NVF). Venting boil-off during the transfer is unnecessary as CHV reduced the wall temperature to the point where boil-off is minimal. The viability of CHV-NVF for tank chilldown in microgravity was demonstrated and was determined to have significant reduction in propellant utilization compared to pure spray cooling at lower pressure. The process was found suitable for microgravity tank chilldown [30].

B. Charge-Hold-Vent to No-Vent-Fill Transition

Tank surface temperature was determined to be the ideal trigger for transitioning between CHV and NVF. Transitioning between CHV and NVF occurs when the tank has been sufficiently chilled to prevent excessive boil-off [31]. To calculate CHV-NVF transition temperature, a program was developed based on the equation derived from Clark and Hartwig [31]. This program is essentially an energy balance between the heat of the fluid and the heat of the wall. Additional information on the equation can be found in Appendix XII.H. Assuming NVF, 2,770,000 liters of cryogenic fluid transferred, a final fill level of 95%, and no parasitic heat leak, the program calculates 141 K and 162 K for methane as the ideal transition temperatures when using CHV-NVF with LOX and LCH₄ respectively. A 0.75% K-type thermocouple measurement error margin will be added to the trigger temperature [30].

An additional challenge is measuring this temperature accurately with a minimal amount of thermocouples. Placing many thermocouples around the tank wall increases the mass, cost, and power requirements. Finding the tank wall regions with the slowest chilldown times reduces the number of thermocouples required. Once those slowest regions reach the trigger temperature, the rest of the tank should also be below that trigger temperature. Structural areas with the largest thermal mass have the longest chilldown times as temperature rises in between CHV charges due to conduction from structural features [30]. Therefore, thermocouples will be placed in these regions.

VII. Cost Analysis

Two cost estimates were generated using NASA's Instrument Cost Model (NICM), providing a cost bound for ECLIPSE. NICM is a JPL cost-modeling tool that uses mass and power-driven Cost-Estimating Relationships (CERs). The cost analysis is derived the sensor properties. The mass and power consumption of pulse flow, microfilm coatings, and CHV-NVF are assumed to be negligible. Taking the sensor's mass range of 15kg-25kg and power of 10W, the lower bound was computed to be \$21.4 million and the higher bound was \$28.6 million. ECLIPSE assumes the high end of this bound. This cost is broken down into \$10 million in Design and Development, \$10.1 million in Fabrication, and \$8.5

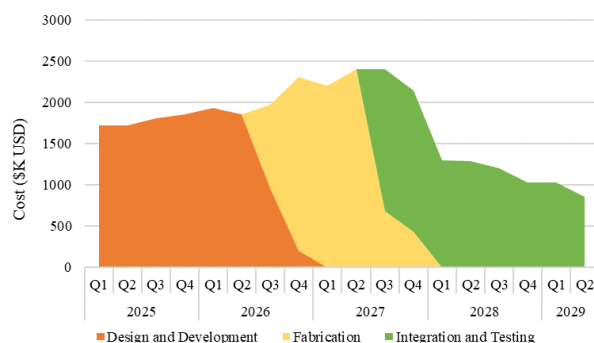


Fig. 13 ECLIPSE Cost Breakdown

million in Integration and Testing. Fig 13 visualizes how the budget is distributed over ECLIPSE's mission timeline.

VIII. Test Campaign

Due to ECLIPSE's aggressive timeline, a special emphasis is placed on integrating reliable cryogenic fluid management technologies that have been demonstrated in microgravity conditions or are gravity independent [3, 30]. However, to achieve the necessary TRL before integration into Artemis 4, a comprehensive validation and verification campaign must be conducted. This campaign will involve multiple microgravity tests designed to address component-level validations and system integration performance metrics.

Pulse flow and the inner transfer line microfilm coating will be tested with an at-scale ground test and then during the protoflight program. As microfilms and pulsed flow have both already been tested in microgravity [3], it is not necessary to repeat those tests simply for verification. The purpose of the at-scale test is to perfect the spray-coating manufacturing process before flight and ensure the larger valve can handle the stresses of pulse flow. The protoflight program will be used to gain more microgravity data for their respective GFSSP models. This data can further improve the heat correlations and improve understanding of pulse flow and microfilm coating's effects on microgravity fluid dynamics. The protoflight program will also be used to test full system integration and work out bugs before it is fully implemented.

To verify the ECLIPSE sensor and to obtain flow regime data points, a standard protoflight program and suborbital flights can be utilized. The standard protoflight program will be leveraged to get more flow regime data points in gravity. As previously mentioned, past research [28] indicates that flow regimes observed in gravity are consistent with those observed under microgravity. Suborbital flights will next be leveraged to obtain additional flow regime data points in the absence of gravity. The limited duration data collected during suborbital flights will be extended using a previously mentioned machine learning-based time-series model, ensuring sufficient data coverage to construct a comprehensive and coherent flow regime identification map.

Lastly, a test campaign is planned for tank chilldown. To accurately trigger the transition from CHV to NVF, a correct estimation of the tank wall's thermal state is needed. This estimation is used to predict the locations with the slowest chilldown time. If thermocouples are not placed at the correct locations, it could result in a failure to fill due to over-pressurization. To mitigate this risk, a testing campaign is proposed to gain a better understanding of the tank's thermal state during CHV.

This testing campaign will consist of parabolic flights that will create data to be used in a simulation of the tank. During this parabolic flight, charges will enter a scale model of the propellant tank and boil-off only during the zero-gravity portions of the flight. While under gravity, the tank will be vented to vacuum. The test tank will have numerous thermocouples evenly distributed across the tank to accurately track the entire tank's thermal state. This general procedure will be repeated until the tank is chilled to cryogenic temperatures throughout. A similar process was done by Chung et al., where they sent in each charge during the 17 seconds of microgravity over five consecutive 80-second parabolas [30]. However, in this campaign, the tank and injector geometry will be made to closely match those of HLS and more thermocouples will be used. This enables the thermal data collected to be more accurate and useful to the HLS mission. This parabolic flight procedure does make some changes to how CHV would work in a real scenario: the array of thermocouples may increase heat leak, and the time in-between parabolas while gravity affects the experiment would not happen in the real situation. Both these changes would exaggerate the effect of parasitic heat leak. While a parabolic flight cannot perfectly map onto a real propellant transfer situation, having any relevant data in microgravity conditions is vital for accurate models.

Following the test of each subsystem of ECLIPSE, a precursor launch is scheduled to test complete system integration. By performing these tests early, ECLIPSE aims to de-risk system integration and identify any potential problems early on. This ensures ECLIPSE's successful implementation into the final launch in the end of FY 2029.

IX. Risk Analysis

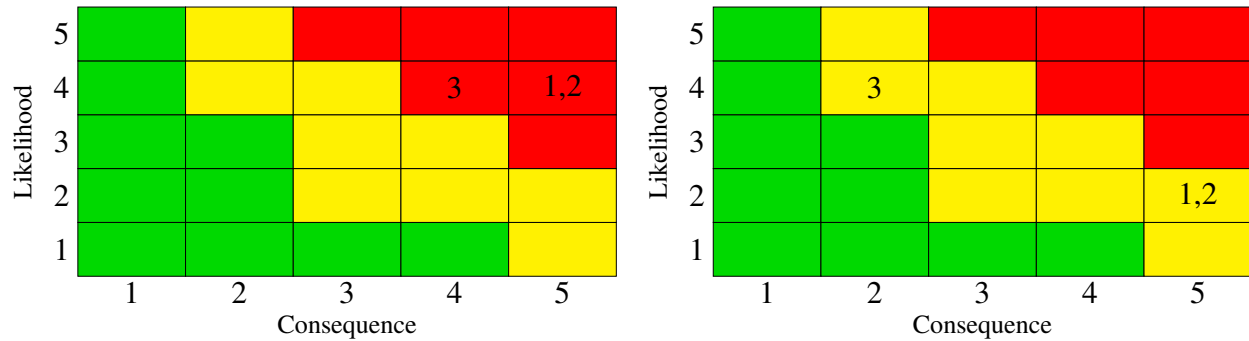


Fig. 14 Pre-Mitigation (Left) and Post-Mitigation (Right) Risk Matrix

ID	Risk	Mitigation
1	Given the lack of verified microgravity cryogenic propellant transfer models, there is a risk associated with uncertainties in heat transfer rates, fluid dynamics, and capacitance measurements, leading to fluctuations in chilldown performance and extra propellant loss.	ECLIPSE’s development timeline incorporates a precursor mission to simulate microgravity conditions, reducing knowledge gaps and validating current chilldown models.
2	The use of modified pulse flow during transfer line chilldown introduces a risk of valve malfunctions, which could disrupt the chilldown process and lead to over-pressurization, causing damage to HLS architecture.	An emphasis will be placed on selecting cryogenic-rated lubricants, implementing valve pre-chill procedures to minimize thermal shock, and conducting rigorous valve cycling tests during testing and integration phase.
3	Given the limited funding for two-phase flow instrumentation, there is a risk resources may be diverted to other cryogenic fluid management technologies. This can increase the cost and timeline span, thereby impacting mission readiness.	The sensor’s gravity-independent measurement technique provides flexibility to leverage existing 1-g research, reducing the need for microgravity experiments and reducing developmental costs.

Table 2 Risk and Mitigation Table

X. Conclusion

From the moment the transfer line is established between the Human Landing System (HLS) and the propellant depot until the completion of single-phase liquid propellant transfer, the ECLIPSE architecture ensures continuous control over the propellant, actively mitigating boil-off and closely monitoring two-phase flow regimes to maintain a smooth and efficient transfer process. ECLIPSE is designed as a comprehensive and minimally invasive transfer solution, fully compatible with all spacecraft variants requiring propellant transfer. To minimize propellant loss during line chilldown, ECLIPSE incorporates pulse flow technology coupled with microfilm-coated transfer lines. Although pulsed flow may introduce hydraulic shock potentially damaging sensitive HLS instrumentation along the transfer line, the team mitigates this risk by optimizing valve closing durations and maximizing chilldown and heat transfer efficiency between the cryogenic fluid and the transfer line. During tank chilldown, ECLIPSE leverages the Charge-Hold-Vent (CHV) and No-Vent-Fill (NVF) operations to minimize tank over-pressurization risks and unintended propellant venting. The CHV-NVF transition is reliably triggered by tank maximum temperature measurements. ECLIPSE further enhances system safety by integrating a precise two-phase flow sensor that monitors and characterizes two-phase flow boiling regimes along the transfer line in real time. This sensor utilizes three statistical parameters derived from time-resolved capacitance measurements, providing detailed insights into flow boiling dynamics. By meeting these design and operational requirements, ECLIPSE directly complies with the 2025 Human Lander Challenge theme requirements, supporting safe and sustainable human exploration far beyond Low Earth Orbit.

XI. Acknowledgments

The team would like to sincerely thank our advisor, Dr. Vishwanath Ganesan, for his guidance and continued support throughout the development of this project. We are extremely grateful to Benjamin Straiton and Matt Charleston from Tech4Imaging for providing technical assistance in the development of ECLIPSE's two-phase flow capacitance sensor. We extend special thanks to Dr. Jason Hartwig of NASA's Glenn Research Center for his critical insights into ECLIPSE's concept, scalability, and logistics, which significantly shaped our system architecture. We are also thankful to Dr. Samuel Darr of The Aerospace Corporation for providing clarity on the inner workings of GFSSP, which enabled the team to develop higher-fidelity models. We greatly appreciate Dr. Andre LeClair for sharing his FORTRAN heat correlation routines, which allowed for accurate modeling of chilldown behavior across various boiling regimes. Finally, we thank former ISS HuLC Project Manager Shikhar Kesarwani, former ISS HuLC Instrumentation Lead Adam Pawlik, and current ISS RASC-AL project manager Benjamin Ochs for their review and feedback on the design.

XII. Appendices

A. Flow Boiling Background

At the beginning of propellant transfer, the connecting tube will be super-heated relative to the cryogenic propellant. Super-heating is the difference in temperature between the tube and liquid boiling point. In a typical space environment, the tubing will cycle between 208K and 398K [32] while cryogenic propellants will be below their boiling temperatures - LH₂: 20K, LOX: 90K, and LCH₄: 111K. To flow liquid between tanks, the tube must first be chilled to cryogenic temperatures. The most efficient way to do this is by using some of the cryogenic propellant as a cooling liquid [3]. However, this technique causes boil-off and reduces available propellant. Mitigating boil-off during line chilldown is therefore a powerful method of increasing the net propellant transferred.

In flow boiling, the temperature difference between the surface and the liquid's boiling point determines boiling characteristics such as heat transfer rate. Film boiling occurs when the super-heating is high, while nucleate boiling occurs when it is lower. In film boiling, a vapor film forms between the liquid and the surface, acting as insulation and significantly reducing heat transfer. In nucleate boiling, bubbles form at nucleation points and transfer heat as they rise through the liquid. Heat flux is up to an order of magnitude higher during nucleate boiling compared to film boiling.

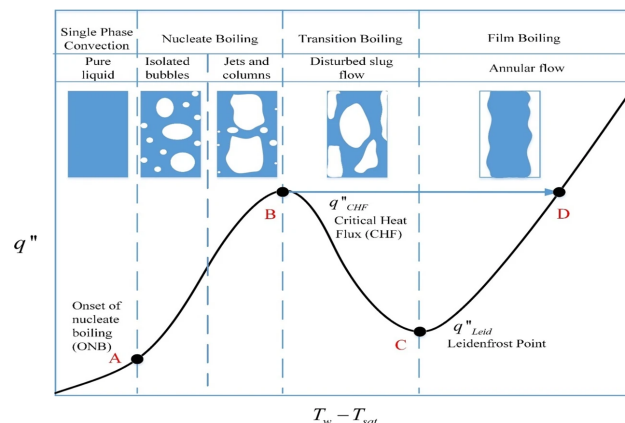


Fig. 15 Typical flow boiling curve [11]

Chilldown efficiency is the ratio of heat removed from the tube, $Q_{removed} [J]$, to the heat of the propellant, $Q_{available} [J]$. Increasing chilldown efficiency effectively reduces the propellant necessary to chill the tubes. This would increase the propellant available for the mission later on, increasing potential payload mass and mission capabilities. Chilldown efficiency can be increased through more thorough vaporization of the propellant. This correlates well with higher heat transfer rates. Chilldown efficiency is defined below.

Equations were source from [12].

$$\eta_{CD} = \frac{Q_{removed}}{Q_{available}} \times 100\% \quad (2)$$

$$Q_{available} = M_{propellant} h_{fg} \quad (3)$$

$$Q_{removed} = M_{tube} c_{tube} \Delta T \quad (4)$$

An estimate of potential propellant savings can be calculated by applying equations (2,3) to to an ideal system with no parasitic heat leak. Let's assume the system consists of a .25m diameter stainless steel tube of length 30m, thickness .025m, and initial temperature -40 C and the chilling fluid is LOX.

$$Q_{removed} = \pi \times .25m \times .025m \times 30m \times 7500 \frac{kg}{m^3} \times 420 \frac{J}{kgK} \times 140K = 259.7MJ$$

With 100% chilldown efficiency, 1200kg of LOX would be needed to chill the tube to cryogenic temperatures. However, conventional methods of chilldown only reach chilldown efficiencies of 8.5% [33]. In this scenario, that efficiency would result in 14,100kg of LOX consumed. Increasing this chilldown efficiency has the potential to save hundreds and even thousands of kilograms of propellant.

B. Hydraulic Shock Background

Hydraulic shock effect is a pressure transient which occurs due to rapid changes in fluid momentum. They typically occur when valves are closed quickly. The kinetic energy of the fluid is converted into potential energy in the form of a pressure wave that travels up and down a line of tubing and approaches zero due to friction. The maximum pressure is modeled by the following equation where ρ , β are fluid properties and D , b , E are the pipes diameter, thickness, and elastic modulus respectively [34].

$$\Delta P = \Delta v \left(\frac{\rho}{1/\beta + \frac{D}{bE} g} \right)^{\frac{1}{2}} \quad (5)$$

Hydraulic shock can be reduced in a variety of ways. Fluid velocity can be reduced, pipe diameter can be increased, or even a pressure spike damper could be added to the system. All of these are overly invasive or increase the mass of the system. The chosen solution for this problem is to increase the valve closure times. A longer valve closing time reduces the rate at which momentum is negated, easing the transition. Specifically, the valve closure time should be longer than τ .

$$\tau = \frac{2L}{a} \quad (6)$$

where a is the speed of sound in the liquid and L is the distance between the pressure source and the valve. When the valve closure time t is longer than τ , the pressure is proportionally reduced.

$$\Delta P_{reduced} = \frac{\tau \Delta P_0}{t} \quad (7)$$

An allowable pressure spike magnitude can be decided based on industry standards. The ASME B31.4 code prohibits the pressure of the system from rising above ten percent of the equilibrium pressure of the system to prevent damage [35]. This pressure spike magnitude applies to either positive or negative pressure fluctuations. Higher pressures can damage system due to greater exerted force while low pressures cause cavitation that also damages components.

C. GFSSP Modeling

Generalized Fluid System Simulation Program (GFSSP) is a NASA-developed software for modeling fluid flow, heat transfer, and phase changes in complex piping networks. GFSSP is used in this paper to model hydraulic shock and the fluid transients that occur during pulse flow. GFSSP has been used for this purpose before and can provide accurate results for the problem.

Many parameters can be adjusted in pulse flow. Pulse length is the amount of time the valve spends open. Duty cycle is the percent of time the valve is open. The type of valve can also affect the closing profile. These parameters can significantly impact the degree with which pulse flow improves efficiency. Figure 16 is an example of pulse flow cross section over time. Typically, ball or butterfly valves are used in propellant feed systems; this analysis uses their closing profiles. Note that it accurately depicts the cross sections during open and close and is not a simple square wave.

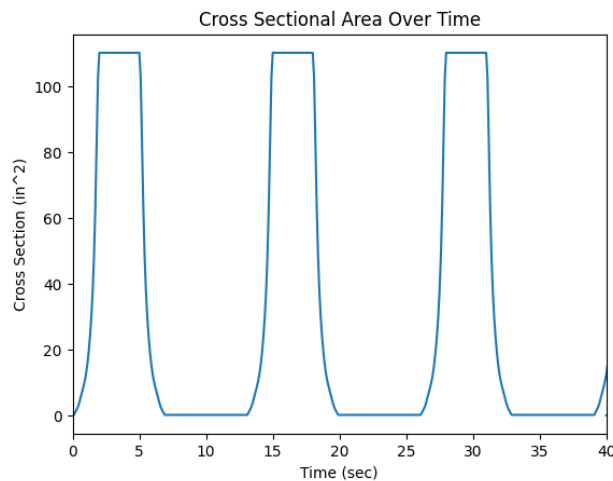


Fig. 16 Example pulse flow ball valve cross section with 3-6 seconds open-closed

Figure 17 depicts the nodal configuration used to create the graphs in Fig. 5. GFSSP has internal nodes and boundary nodes with branches between them. A valve can be simulated by adjusting the cross section of a restriction. The nodal configuration below connects the first boundary node, a liquid cryogenic tank, to the final boundary node, the atmosphere, with piping and a valve. This is a relatively simple configuration that is used as a proof of concept for the chosen method of pressure spike mitigation. A total length of 40 ft, a pipe inner diameter of 10 in, inlet pressure of 100 psi, and outlet pressure of 14.7 psi were used in this configuration.

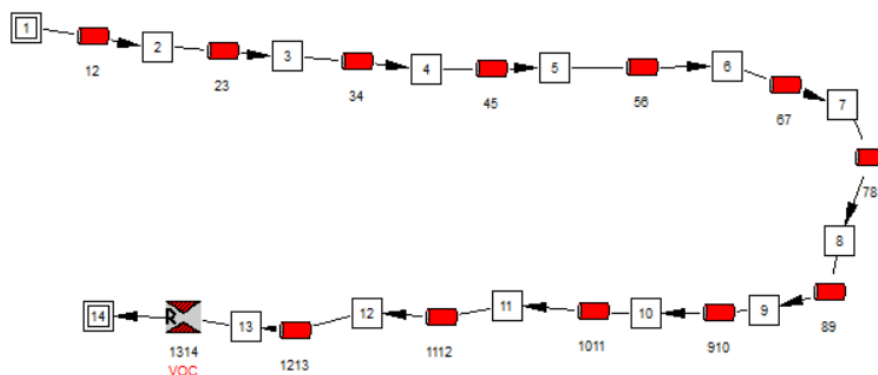


Fig. 17 Simple nodal configuration to proof concept

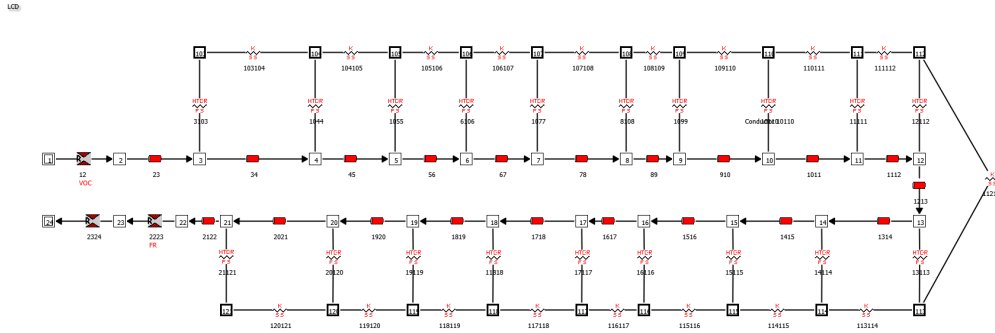


Fig. 18 Line chilldown model was based on LeClair's work and used to simulate pulse flow chilldown.

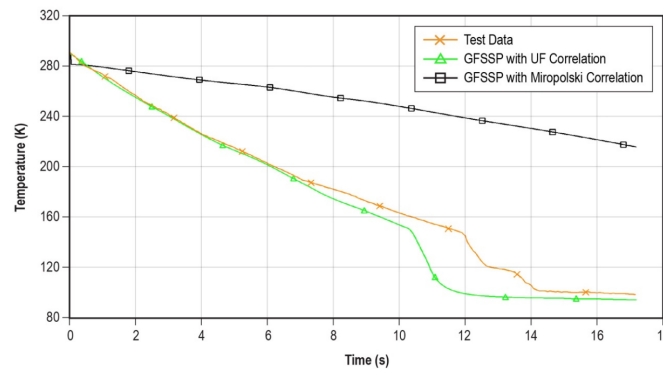


Fig. 19 Upstream node chilldown from LeClair, with mean inlet Re of 68,200 [7].

Figure 18 depicts a nodal configuration which represents the chilldown process. This configuration was modeled after the configuration in [7]. The model has a 0.46 in inner diameter, 0.50 in outer diameter, 22.5 in length, and uses Stainless Steel 304 as the pipe material. The simulation utilized a 0.005 s timestep with a flow regulator at restriction 2223 to match measured flow rates from LeClair [7]. The valve open-close was placed at restriction 12. An inlet pressure of 23 psi and outlet pressure of 20 psi was used. This model includes conjugate heat transfer to simulate the chilling of the tube mass. Heat correlations were obtained from Dr. LeClair to match data from [8] and model proper heat transfer in the film boiling, transition boiling, and nucleate boiling flow regimes. The correlations modeled both zero-g and 1-g heat transfer.

Before conducting variations on the original experiment from LeClair, the model was compared to the original experiment's results to validate its development. Figure 19 represents the line chilldown times for the upstream node, defined as node 107, for a model with a mean Re of 68,200. The model developed had a mean Re of 41,300 due to slower mass flow rates and therefore has a slightly longer chilldown time, which is consistent with the results from [7]. This result is available in Figure 20.

Figure 21 depicts the nodal model used to model the effect of microfilm coatings on line chilldown. This model was also based on LeClair's work [7] and was adjusted to simulate microfilm coatings. The first set of solid nodes represents the microfilm coating and used heat transfer coefficients from NIST [16]. The second set of solid nodes represents the bulk mass of the tube. A diameter of 0.46 in and total tube length of 22.5 in was used. An inlet pressure of 23 psi and outlet of 20 psi was used.

Further research was conducted on the differences in line chilldown caused by 1-g and 0-g. Figure 22 represents the chilldown times for both models with continuous flow, and figure 23. The 0-g heat correlations were provided by Dr. LeClair and based upon [8]. These graphs demonstrate similar line chilldown and validate pulse flow in microgravity.

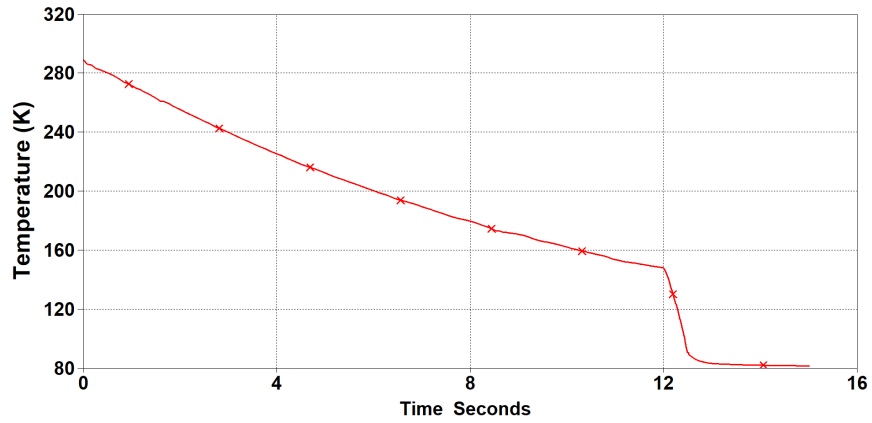


Fig. 20 Upstream node chilldown developed model, with mean inlet Re of 41,300

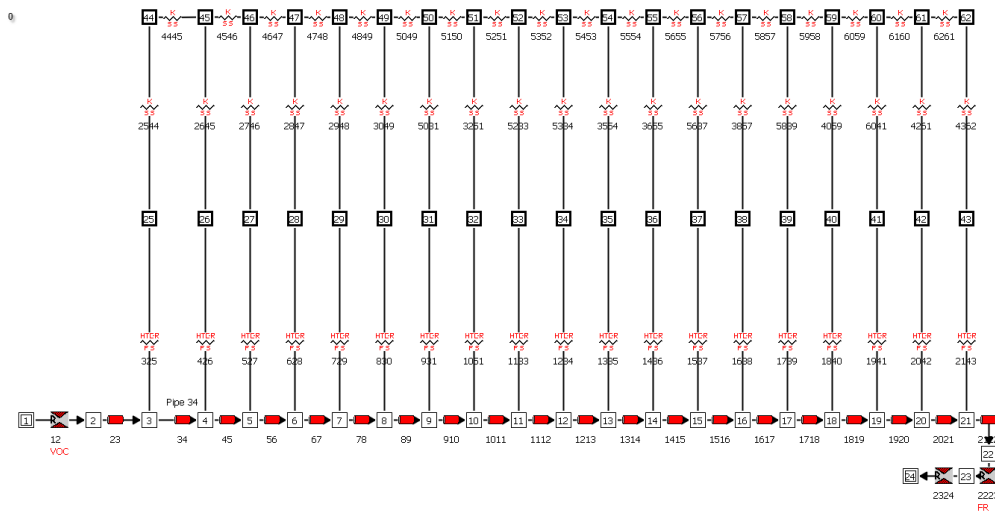


Fig. 21 Nodal model used to simulate microfilm coating chilldown in GFSSP. The two sets of solid nodes represent the coating and then the bulk tube.

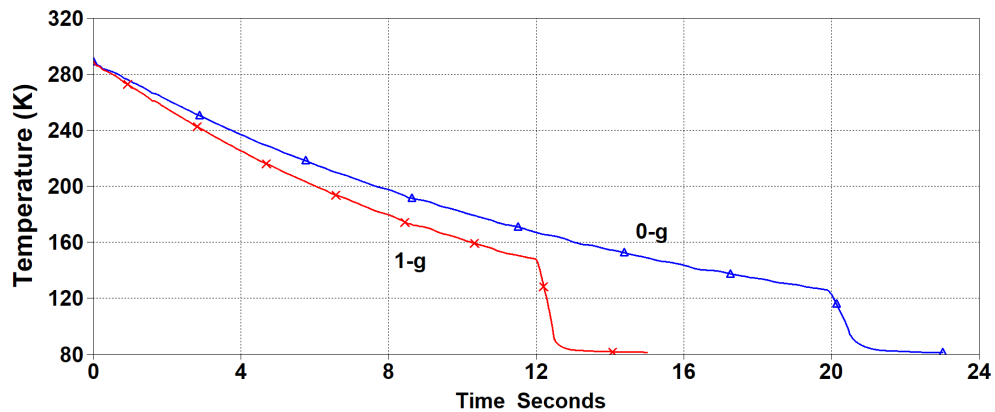


Fig. 22 Line chilldown time 1-g vs 0-g for the upstream node

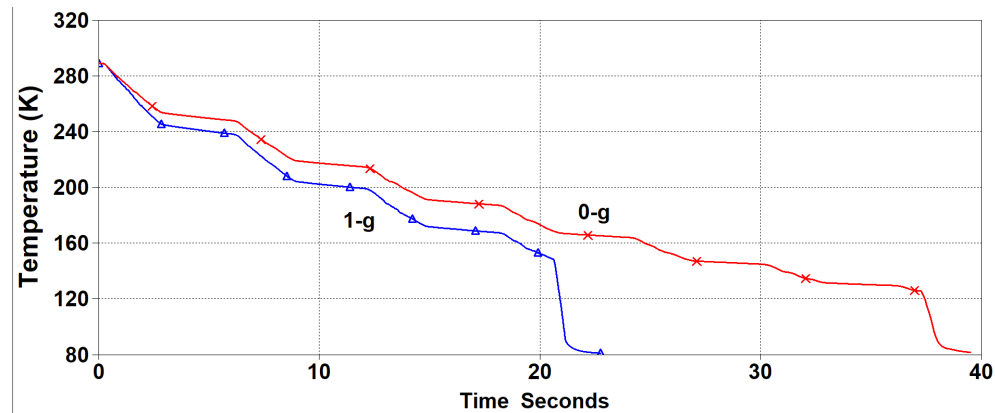


Fig. 23 Pulse line chilldown time 1-g vs 0-g for the upstream node with 1 second valve open and 3 second valve close

D. Tube Modification Trade Study

Microfilm coatings promote earlier nucleate boiling by insulating the liquid from the surface with a low-conductivity layer. Micro-fins destabilize the vapor film boundary with periodic fins. Capillary coatings use capillary forces to maintain fluid-surface contact in micro-channels. Surface etching and micro-structures increase the surface area and can be optimized with specific patterns and have various methods of manufacture. Many of these modifications are prone to wearing down due to their extrusions into flowing, turbulent fluids. Moreover, while some options provide a very large increase in heat transfer and boil-off reduction, they have only been made in laboratory settings at a small scale.

Microfilm Coating Additional Information

Microfilms are the chosen tube modification for propellant transfer. They greatly enhance chilldown efficiency and have the most advanced TRL and MRL levels [11]. Moreover, they provide little change to the continuous flow and likely have the lowest risk of degrading over time. Fig. 24 depicts a tube with microfilm coating.

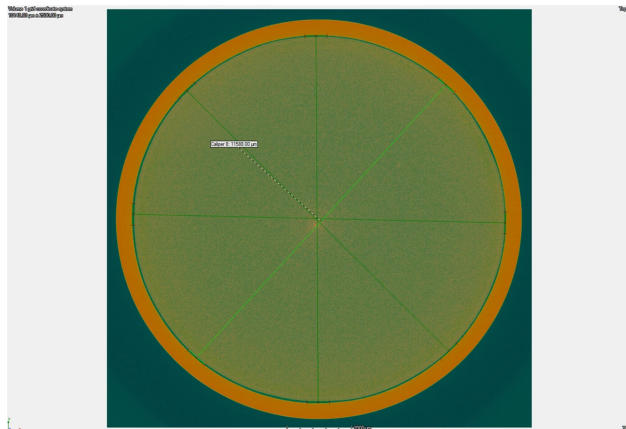


Fig. 24 X-ray tomography of a pipe with microfilm coating

Eq. 8 estimates the coating mass per length of tube.

$$M = \frac{\pi l(D^2 - d^2)}{4} \frac{\rho}{.003785m^3} \quad (8)$$

where l is the length of the tube, D is the diameter of the tube, d is the interior diameter of the tube after coating, and ρ is the density of the coating in lbs/gallon.

The coating can be applied any number of times to increase the layer count, though excessive coatings provides insulation which reduces the heat transfer rate. Additional coatings would also increase the added mass and time and cost to manufacture.

Micro-fins Additional Information

Micro-fins are small structures that are placed on the inside of the transfer pipe. These fins enhance heat transfer by disturbing the flow layers[36]. Although this greatly increases heat transfer it a significant increases in pressure. Due to these problems along with a low TRL and durability concerns, micro-fins were rejected.

Capillary Coatings Additional Information

Capillary coatings are a porous layer that can be applied inside cryogenic tubes that use capillary action to draw liquid along the heated surface which in return significantly enhances heat transfer[37]. However, this coating has not been widely tested and researched for cryogenics applications and is prone to corrosion and breakage.

Surface Etching Additional Information

Surface Etching can be done with chemical or laser etching. Both create a textured pattern that enhances heat transfer[38]. Due to the nature of these etched patterns, there are significant concerns of wear that will cause loss of chill down efficiency overtime.

Microstructure Additional Information

Micro-structures are specially fabricated microscopic patterns formed by TBAF and UV curing that enhance heat transfer by altering the contact with the liquid and liquid vapor within the tube[39]. This tube modification is difficult to manufacture and there has not been widely applied with cryogenics.

Trade Matrix

Table 3 summarizes the trade study conducted to choose the optimal tube modification. It contains the real values found for each item. Table 4 summarizes the weighted totals of each tube modification. While microfilms lack in heat transfer enhancement, their high scores in all other categories make them an optimal choice.

Item	Microfilm Coating	Microfins	Capillary Coatings	Surface Etching	Microstructures
Technology Readiness Level (TRL)	7	5	3	5	3
Manufacturing Readiness Level (MRL)	8	4	2	4	3
Heat Transfer Enhancement (% Over Bare)	109.1	60	250	104	500
Pressure Fluctuation (% Difference)	0	136	0	65	0
Durability	10	3	5	5.5	4

Table 3 Unweighted Trade Matrix Values

Item	Microfilm Coating	Microfins	Capillary Coatings	Surface Etching	Microstructures	Weight
Technology Readiness Level	1	0.71	0.43	0.71	0.43	0.15
Manufacturing Readiness Level	1	0.5	0.25	0.5	0.375	0.15
Heat Transfer Enhancement	0.22	0.12	0.5	0.21	1	0.2
Pressure Fluctuation	0	1	0	0.48	0	-0.1
Durability	1	0.3	0.5	0.55	0.4	0.15
Total	0.494	0.1505	0.277	0.258	0.38075	

Table 4 Weighted Tube Modification Matrix

E. Asymmetrical Sensor Visualization

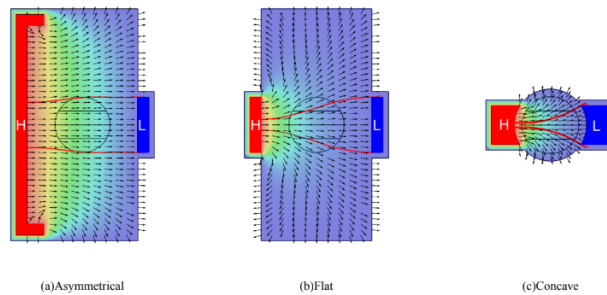


Fig. 25 Visualization of Each Type

F. Sensor Parameters

The excitation frequency (which is the frequency of the applied a.c. voltage to the sensor) is a sine-wave applied between the sensor electrodes. This is set to 10 Hz, a frequency safely above the flow characteristic frequency of a 10 inch cryogenic line which is > 1 Hz. Note, the flow characteristic frequency is a property of the cryogenic pipe, and is defined as the frequency where the magnitude of the displacement current and the conduction current (current generated in the cryogenic line) are the same. Setting the excitation frequency to be an order of magnitude above the flow characteristic frequency minimizes potential inaccuracies in the measured capacitance signal. The system power of the sensor is to be set to 10 watts, which is a reasonable number since capacitance sensing inherently requires low power [40]. The potential difference of the electrodes was found to be 25 V, after scaling up the potential difference from a smaller pipe diameter [24].

G. Sensor Accuracy Adjustment in Cryogenic Temperatures

At such low temperatures in cryogenic environments, the capacitance sensor performance can be altered due to thermal contraction of the materials of its electrical components and variations in the permittivity of gases and liquids. For example, as the temperature decreases, the contraction of sensor components can alter their geometry, while shifts in fluid permittivity affect the electric field distribution within the sensor. The work of [20] analyzes how cryogenic temperatures lead to deviations in capacitance measurements. Figure 8a from [20] illustrates these effects where in multiple tests, after opening the flow distribution valve to the end of the chill, the initial void fraction is 100%, but the final void fraction falls slightly below 100%.

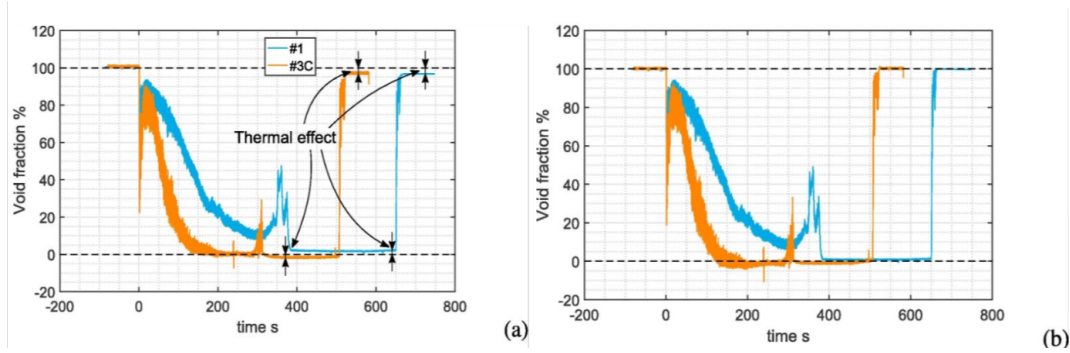


Fig. 26 Void fraction time histories before (a) and after (b) the “thermal effect” correction.

To address these challenges, several mathematical equations were developed that describe thermal contraction and permittivity variations.

$$\Delta L = L_0 \alpha \Delta T \quad (9)$$

The thermal contraction equation above predicts the dimensional changes in the sensor components, where ΔL represents the change in material length, L_0 represents the initial length, α represents the thermal expansion coefficient and ΔT represents the temperature change.

$$\epsilon_g = 1 + A_g \frac{P}{T} \quad (10)$$

$$\epsilon_l = A_l + \frac{B_l}{T} \quad (11)$$

Similarly, variations in permittivity were modeled using equations specific to gases (ϵ_g) and liquids (ϵ_l), where A_g , A_l , B_l are material-specific constants, P is pressure, and T is temperature.

The graphical data in fig. 26 from [20] emphasizes the importance of accounting for these thermal effects. The plots show that both the thermal contraction and permittivity variations contribute to measurable deviations in the sensor outputs. However, the sensor becomes less accurate in highly unstable two-phase flow. Additionally, the equations assume that the fluid temperature is equal to the wall temperature.

H. Tank Chardown Temperature Transition Calculation

The team developed a Python program to calculate the ideal temperature to transition between CHV and NfV. The program utilizes equation 12 and evaluates an ideal transition temperature, as used in [31]. The equation states that the energy lost by the tank and parasitic heat into the tank is equivalent to the energy absorbed by the fluid. The calculated temperature is maximum temperature the tank can be for a safe NfV. The temperature used should be lower than this by a safety margin to account for possible error.

$$\begin{aligned} m_{\text{fluid,final}} u_{\text{fluid,final}} - (m_{\text{liquid,initial}} u_{\text{liquid,initial}} + m_{\text{vapor,initial}} u_{\text{vapor,initial}}) \\ - (m_{\text{fluid,final}} - m_{\text{fluid,initial}}) h_{\text{inlet}} = \dot{Q}_{\text{para,avg}} \Delta t - m_{\text{tank}} \int_{T_{\text{initial}}}^{T_{\text{final}}} C_{\text{tank}} dT \end{aligned} \quad (12)$$

The subscript 'fluid' represents the combined liquid and vapor at the end of the transfer. t represents time, T represents temperature, m represents mass (kg), u is internal energy (J/kg), C is specific heat (J/kg*K), h_{inlet} is specific inlet enthalpy (J/kg), and \dot{Q} is the heat transfer rate (W), The separate initial liquid and vapors terms represents residue fluid in the receiving tank from CHV.

I. Sensor Materials Trade Matrix

Material	Ceramic Fiber	Alumina	Aerogel	X-Aerogel
Cost (\$/lb)	12.64	5.93	23,000	18,000
Density (kg/m^3)	96	3600	0.075	50
Thermal Insulation (R-value)	3.75	12	10.3	20
Dielectric constant	3.55	9.4	1	1.4
Compressive Strength (PSI)	78	296,000	23	30,000
MRL	10	10	9	6

Table 5 Insulator Materials Trade Matrix

Criterion	Weight	Ceramic Fiber	Alumina	Aerogel	X-Aerogel
Cost	-0.10	0.0005	0.0002	1	0.78
Density	-0.10	0.027	1	0.00002	0.014
Thermal Insulation	0.20	0.18	0.6	0.52	1
Dielectric Constant	-0.10	0.38	1	0.11	0.15
Compressive Strength	0.15	0.0002	1	0.00007	0.10
MRL	0.10	1	1	0.9	0.6
Total		0.0952	0.170	0.0830	0.1806

Table 6 Weighted Materials Trade Matrix

Criterion	Aluminum	Copper
Cost (\$/lb)	1.12	4.32
Density ($kg\ m^{-3}$)	2700	8920
Skin Depth @ 1 MHz (μm)	82	65
Electrical Conductivity (% IACS)	59	100
Specific Strength ($MPa\cdot cm^3/g$)	115	25
Corrosion Rating (1–10)	8	6
Machinability Index (% B1112)	270	20

Table 7 Shield-Material Trade Matrix

Criterion	Weight	Aluminum	Copper
Cost	-0.12	0.26	1.00
Density	-0.14	0.30	1.00
Skin Depth	-0.20	1.00	0.79
Electrical Conductivity	0.35	0.59	1.00
Specific Strength	0.15	1.00	0.22
Corrosion Rating	0.10	1.00	0.75
Machinability Index	0.10	1.00	0.07
Total		0.283	0.047

Table 8 Weighted Shield-Material Trade Matrix

J. ANSYS Simulation Parameters

This simulation serves as a preliminary proof of concept for transient multiphase flow modeling in a cryogenic propellant transfer line. The configuration and parameters are outlined below.

Mesh Configuration

Both the pipe and fluid domains are fully meshed to enable future investigations of heat transfer phenomena. The mesh consists of 227,561 nodes and 971,603 elements, approaching the upper limit allowed by the student license. A swept mesh strategy is employed, with a free mesh on the seed face that accommodates both quadrilateral and triangular elements, which are then extruded along the cylinder axis. At this stage, no inflation layers are present at the wall, but these can be introduced in subsequent simulations to improve near-wall resolution and accuracy.

Solver and Model Settings

The simulation utilizes a pressure-based solver with an operating pressure set to zero Pascals. The Eulerian multiphase model is selected to effectively capture mixtures with significant phase volume fractions. Oxygen gas is designated as the primary phase, while liquid oxygen serves as the secondary phase. Mass phase interactions, specifically evaporation and condensation, are modeled using the Lee model with default parameters. Energy modeling is enabled to allow for the possibility of simulating heat transfer between the fluid and the pipe. The SST k-omega turbulence model is applied using mixture properties, and all other solver settings are maintained at their default values. The simulation is transient (unsteady), using a first-order implicit time discretization.

Material Properties

Material definitions for liquid oxygen and oxygen gas are sourced from the ANSYS materials database. In order to better reflect the expected physical behavior under operational conditions, it may be preferred to model oxygen gas as an incompressible ideal gas, rather than with constant density.

Boundary Conditions

A no-slip condition is enforced at all wall boundaries. Liquid oxygen is introduced through a velocity inlet, with the velocity adjusted to control the progression through different flow regimes. The inlet velocity for liquid oxygen is 1 m/s at 300 K, and for oxygen gas it is 0 m/s at 300 K. The volume fraction for liquid oxygen at the inlet is 1. This inlet condition is expected to be updated to a pressure inlet in future iterations. The thermal boundary condition at the inlet is set to 300 K, but this parameter can be further optimized. The wall is made of aluminum with a heat flux of 0 W/mm².

Solution Controls and Output

Standard initialization procedures are used for the simulation. The time step length is 0.01 seconds and the total number of time steps is 990. These are evaluated with ongoing adjustments to optimize transient resolution and computational efficiency. The simulation outputs include phase volume fraction data and animations of volume fraction contours along a plane containing the fluid domain axis.

K. Code

All the simulations code done in this technical paper can be found in https://github.com/ISSUIUC/HuLC_2025_UIUC.



References

- [1] Hansen, H. C., Johnson, W. L., Meyer, M., Werkheiser, A., and Stephens, J. R., “Cryogenic fluid Management technologies enabling for the Artemis program and beyond,” *ASCEND 2022*, 2020. <https://doi.org/10.2514/6.2020-4000>.
- [2] Johnson, W. L., and Stephens, J. R., “NASA’s Cryogenic Fluid Management Technology development Roadmaps,” , 8 2018. URL <https://ntrs.nasa.gov/citations/20190000305>.
- [3] Jason Hartwig, J. D. B. H. H. W. S. D. M. T. S. J. M. D., J. N. Chung, “Nitrogen flow boiling and chilldown experiments in microgravity using pulse flow and low-thermally conductive coatings,” *Nature Microgravity*, Vol. 8, No. 33, 2022. <https://doi.org/10.1038/s41526-022-00220-9>.
- [4] J.N. Chung, H. W. S. D. J. H., Jun Dong, “Enhancement of convective quenching heat transfer by coated tubes and intermittent cryogenic pulse flows,” *International Journal of Heat and Mass Transfer*, Vol. 141, 2019.
- [5] Shaeffer, R., “Cryogenic Chilldown with Pulse Flow Liquid Nitrogen,” , 2012. Undegraduate Honors thesis from the University of Florida.
- [6] A.K. Majumdar, R. M. P. S., A.C. LeClair, *Generalized Fluid System Simulation Program, Version 6.0, User Manual*, March 2016. NASA/TP-2016-218218.
- [7] LeClair, A., “Modeling Cryogenic Chilldown of a Transfer Line with the Generalized Fluid System Simulation Program,” 2018. URL <https://www.nasa.gov/wp-content/uploads/2024/04/gfssp-ln2andlh2chilldown-aiaa2018.pdf?emrc=66201987b71df>.
- [8] Darr, S. R., Hartwig, J. W., Dong, J., Wang, H., Majumdar, A. K., LeClair, A. C., and Chung, J. N., “Two-Phase Pipe Quenching Correlations for Liquid Nitrogen and Liquid Hydrogen,” *Journal of Heat Transfer*, Vol. 141, No. 4, 2019, p. 042901. <https://doi.org/10.1115/1.4041830>, URL <https://doi.org/10.1115/1.4041830>.
- [9] AK Majumdar, R. F., “Numerical Modeling of Fluid Transients by a Finite Volume Procedure for Rocket Propulsion Systems,” *Volume 1: Fora, Parts A, B, C, and D*, 2003.
- [10] Takeda, D., Fukiba, K., and Kobayashi, H., “Improvement in pipe chilldown process using low thermal conductive layer,” *International Journal of Heat and Mass Transfer*, Vol. 111, 2017, pp. 115–122. <https://doi.org/https://doi.org/10.1016/j.ijheatmasstransfer.2017.03.114>, URL <https://www.sciencedirect.com/science/article/pii/S0017931016335773>.
- [11] J. N. Chung, H. W. S. D. J. W. H., Jun Dong, “An advance in transfer line chilldown heat transfer of cryogenic propellants in microgravity using microfilm coating for enabling deep space exploration,” *Nature Microgravity*, Vol. 7, No. 21, 2021. <https://doi.org/10.1038/s41526-021-00149-5>.
- [12] Chung, J., Darr, S., Dong, J., Wang, H., and Hartwig, J., “Heat transfer enhancement in cryogenic quenching process,” *International Journal of Thermal Sciences*, Vol. 147, 2020, p. 106117. <https://doi.org/10.1016/j.ijthermalsci.2019.106117>.
- [13] Barhoumi, N., Khelifi, K., Maazouz, A., and Lamnawar, K., “Fluorinated Ethylene Propylene Coatings Deposited by a Spray Process: Mechanical Properties, Scratch and Wear Behavior,” *Polymers*, Vol. 14, No. 2, 2022. <https://doi.org/10.3390/polym14020347>, URL <https://www.mdpi.com/2073-4360/14/2/347>.
- [14] Plastics, P., “FEP vs PTFE: Fluoropolymer Comparison,” 2024. URL [https://www.pbyplastics.com/blog/decoding-fluoropolymers-a-comprehensive-comparison-of-fep-vs-ptfe#:~:text=PTFE%27s%20higher%20maximum%20temperature%20makes,of%20thermal%20expansion%20\(CTE\)](https://www.pbyplastics.com/blog/decoding-fluoropolymers-a-comprehensive-comparison-of-fep-vs-ptfe#:~:text=PTFE%27s%20higher%20maximum%20temperature%20makes,of%20thermal%20expansion%20(CTE)).
- [15] Curbell Plastics, D. K. H., Inc, “DESIGN CONSIDERATIONS FOR THE USE OF PLASTIC MATERIALS IN CRYOGENIC ENVIRONMENTS,” 2014. URL https://www.curbellplastics.com/wp-content/uploads/2022/11/Plastic-Materials-in-Cryogenic-Environments.pdf?srltid=AfmBOooJWsoGSRcV-MAGoKQucUByw53DoOVLhMY97zWXoA35iI_IF3rO.
- [16] NIST, “Material Properties: Teflon,” , 2025. URL https://trc.nist.gov/cryogenics/materials/Teflon/Teflon_rev.htm.
- [17] Filippov, Y. P., and Alexeyev, A. I., *Improvement of Radio Frequency Void Fraction Sensors*, Springer US, Boston, MA, 1994, pp. 1097–1104. https://doi.org/10.1007/978-1-4615-2522-6_134, URL https://doi.org/10.1007/978-1-4615-2522-6_134.
- [18] Nassos, G. P., “DEVELOPMENT OF AN ELECTRICAL RESISTIVITY PROBE FOR VOID-FRACTION MEASUREMENTS IN AIR-WATER FLOW,” Tech. rep., Northwestern Univ., Evanston, IL (United States); Argonne National Lab., Ill.; Associated Midwest Universities, Lemont, Ill., 1963. <https://doi.org/10.2172/4664104>, URL <https://www.osti.gov/biblio/4664104>.
- [19] Berthold, J., Reed, S., and Nash, C., “Fibre optic sensor system for void fraction measurement in aqueous two-phase fluids,” *Flow Measurement and Instrumentation*, Vol. 5, No. 1, 1994, pp. 3–13. [https://doi.org/https://doi.org/10.1016/0955-5986\(94\)90003-5](https://doi.org/https://doi.org/10.1016/0955-5986(94)90003-5), URL <https://www.sciencedirect.com/science/article/pii/0955598694900035>.



- [20] Yuki Sakamoto, H. K. T. S., Laura Peveroni, and Johan Steelant, J.-M. B., “Void fraction measurement in cryogenic flows. Part II: Void fraction capacitive sensor performances in chilldown experiments,” *Cryogenics*, Vol. 96, 2018, pp. 25–33. <https://doi.org/10.1016/j.cryogenics.2018.10.002>.
- [21] Canière, Hugo, “Flow pattern mapping of horizontal evaporating refrigerant flow based on capacitive void fraction measurements,” Ph.D. thesis, Ghent University, 2009. URL http://lib.ugent.be/fulltxt/RUG01/001/367/313/RUG01-001367313_2010_0001_AC.pdf.
- [22] Kim M, J. J. O. M. S. T. S. K., Komeda K, “Optimizing Calibration for a Capacitance-Based Void Fraction Sensor with Asymmetric Electrodes under Horizontal Flow in a Smoothed Circular Macro-Tube,” *Sensors*, 2022.
- [23] Libert, N., Morales, R. E., and da Silva, M. J., “Capacitive measuring system for two-phase flow monitoring. Part 2: Simulation-based calibration,” *Flow Measurement and Instrumentation*, Vol. 50, 2016, pp. 102–111. <https://doi.org/https://doi.org/10.1016/j.flowmeasinst.2016.05.011>.
- [24] Yuki Sakamoto, H. K., Tetsuya Sato, “Development study of a capacitance void fraction sensor using asymmetrical electrode plates,” *Journal of Fluid Science and Technology*, Vol. 11, No. 2, 2016, pp. JFST0008–JFST0008. <https://doi.org/10.1299/jfst.2016jfst0008>.
- [25] Broesch, J. D., “Chapter 4 - The Math of DSP,” 2009, pp. 37–80. <https://doi.org/https://doi.org/10.1016/B978-0-7506-8976-2.00004-3>, URL <https://www.sciencedirect.com/science/article/pii/B9780750689762000043>.
- [26] Jedediah M. Storey, M. T. E. S. C., Brandon S. Marsell, “Propellant Mass Gauging in Microgravity with Electrical Capacitance Tomography,” Tech. rep., National Aeronautics and Space Administration, 2023.
- [27] v. Balakotaiah, Jayawardena, S. S., and Nguyen, L. T., “Studies on Normal and Microgravity Annular Two Phase Flows,” ??? URL <https://ntrs.nasa.gov/api/citations/20010004266/downloads/20010004266.pdf>.
- [28] Bousman, W. S., “Studies of Two-Phase Gas-Liquid Flow in Microgravity,” *NTRS - NASA Technical Reports Server*, 1995. URL <https://ntrs.nasa.gov/archive/nasa/casi.ntrs.nasa.gov/19950018486.pdf>.
- [29] J. N. Chung, H. W. S. R. D. J. W. H., Jun Dong, “Cryogenic spray quenching of simulated propellant tank wall using coating and flow pulsing in microgravity,” *NPJ microgravity*, 2022. <https://doi.org/10.1038/s41526-022-00192-w>.
- [30] J. N. Chung, H. W. B. H. H. J. H., Jun Dong, “Demonstration of charge-hold-vent (CHV) and no-vent-fill (NVF) in a simulated propellant storage tank during tank-to-tank cryogen transfer in microgravity,” *Nature Microgravity*, Vol. 10, No. 64, 2024. <https://doi.org/10.1038/s41526-024-00403-6>.
- [31] Clark, J., and Hartwig, J., “Assessment of prediction and efficiency parameters for cryogenic no-vent fill,” *Cryogenics*, Vol. 117, 2021, 103309. <https://doi.org/10.1016/j.cryogenics.2021.103309>.
- [32] Plante, J. L., “Environmental Conditions for Space Flight Hardware: A Survey,” NASA, 2005.
- [33] Hartwig, J., Chung, J., Darr, S., Wang, H., Huang, B. H., Dong, J., Jain, S., Taliaferro, M., and Doherty, M., “The effect of gravity on cryogenic transfer line chilldown performance using pulse flow and low thermally conductive coatings,” *International Journal of Heat and Mass Transfer*, Vol. 216, 2023, p. 124549. <https://doi.org/10.1016/j.ijheatmasstransfer.2023.124549>.
- [34] Britton, Laurence, W. R., “Avoiding water hammer and other hydraulic transients,” *Process Safety Progress*, 2023.
- [35] Prentice, W., “Understand and Mitigate Waterhammer in Fluid Processes,” 2021.
- [36] Lei Wang, X. H. S. H. M. Y. L. G. L., Jiaojiao Wang, “Experimental investigation on cryogenic chilldown performance under high-Reynolds number condition and using interior micro-fin structure,” *International Journal of Heat and Mass Transfer*, Vol. 182, 2022, p. 121979. <https://doi.org/10.1016/j.ijheatmasstransfer.2021.121979>.
- [37] Surtaev, A., Pavlenko, A., Kuznetsov, D., Kalita, V., Komlev, D., Ivannikov, A. Y., and Radyuk, A., “Heat transfer and crisis phenomena at pool boiling of liquid nitrogen on the surfaces with capillary-porous coatings,” *International Journal of Heat and Mass Transfer*, Vol. 108, 2017, pp. 146–155. <https://doi.org/10.1016/j.ijheatmasstransfer.2016.11.100>.
- [38] Mohamed H. Mousa, R. R. V. G. S. K. C.-M. Y. K. F. R. N. V. U. K. N. N. M., Md Rakibul Hasan Roni, “Water flow boiling heat transfer and pressure drop in smooth, etched, and herringbone aluminum tubes,” *Applied Thermal Engineering*, Vol. 257, 2024, p. 124426. <https://doi.org/10.1016/j.applthermaleng.2024.124426>.

- [39] Graffiedi, M., and Dent, K. S. B. M., Francis J., “Cryogenic quenching process enhancement through coating and microstructure optimization,” *Journal of Physics: Conference Series*, Vol. 2766, No. 1, 2024, p. 012139. <https://doi.org/10.1088/1742-6596/2766/1/012139>.
- [40] Puers, R., “Capacitive sensors: When and how to use them,” *Sensors and Actuators A: Physical*, Vol. 37-38, 1993, pp. 93–105. [https://doi.org/https://doi.org/10.1016/0924-4247\(93\)80019-D](https://doi.org/https://doi.org/10.1016/0924-4247(93)80019-D), URL <https://www.sciencedirect.com/science/article/pii/092442479380019D>, proceedings of Eurosensors VI.

